Reservoir quality and sedimentology in shallow marine sandstones: interplay between sand accumulation and carbonate and clay minerals

Dinfa Vincent Barshep and Richard Henry Worden.*

University of Liverpool, School of Earth Ocean and Ecological Sciences, Herdman Building, L69 3GP

*Corresponding author: Richard Henry Worden, University of Liverpool, School of Earth Ocean and Ecological Sciences, Herdman Building, L69 3GP

Email: rworden@liverpool.ac.uk

ABSTRACT

Sedimentological studies are important in understanding and predicting reservoir quality, especially in shallow buried sandstones that are dominated by eogenetic processes. Understanding the sedimentological controls on siliciclastic depositional environments will enhance the knowledge and prediction of reservoir architecture and reservoir quality, both of which are essential to resource exploitation and future CCS and hydrogen storage projects. Here, we present a study of sedimentology and depositional mineralogy, as well as controls on the deposition of siliciclastic sandstones, from the shallow-buried, Upper Jurassic Corallian marine sandstones of the Weald Basin, UK. These sandstones host small oil accumulations and, being close to large centres of population, are possible gas storage or carbon capture and storage sites. We used wireline log analysis, high resolution core logging, optical petrography, and SEM-EDS imaging to investigate reservoir architecture and the relative importance of depositional versus secondary diagenetic controls on reservoir quality. Shallow marine conditions, adjacent to a continent experiencing a warm humid climate, are interpreted based on ichnofabrics and mineralogy. Tectonic processes influenced water depth which subsequently controlled both the quantity of detrital bioclastic material (and the resulting calcite cement), and the amount of detrital clay matrix. The eustatic influence on deposition led to the development of a relatively thin intra-Corallian mudstone which compartmentalises the reservoir into discrete upper and lower sand bodies. The results of this study underline the importance of integration of detailed sedimentological and wireline log analysis in improving the prediction of reservoir quality in tectonically active environments for shallow buried, eogenetic-dominated sandstones.

Keywords:

Weald Basin, Corallian sandstone, transgressive sandstones, reservoir quality prediction, eodiagenesis, tectonism, wireline log lithology

1. Introduction

Siliciclastic shallow-marine environments are one of the settings that mark the boundaries between continent and ocean. The transient nature of the boundaries between continent and ocean is due to the interplay of the mechanisms that control deposition, including relative sea level, tectonic processes such as fault movement, sediment flux and climate (Andrieu et al., 2016; Burton et al., 1987; Dailly, 1975; Lawrence, 1993; Posamentier and Vail, 1988; Wagoner et al., 1990). The interplay of these four controls produces a wide range of possible depositional sedimentological characteristics (Kupecz et al., 1997; Walker and James, 1992) which in turn control reservoir quality, especially in shallow buried reservoir rocks (Worden et al., 2018). It follows that reservoir quality prediction must involve sedimentological analysis of primary sand characteristics as well as petrophysical analysis of the effects of diagenetic processes and their evolution with time during burial, compaction and heating (Kupecz et al., 1997).

Many studies have applied depositional mineralogy, facies and facies associations as key elements to unlock an appreciation of the depositional controls on reservoir quality (Rahman and Worden, 2016; Schmid et al., 2004). Some studies have also considered the effects of primary depositional controls on reservoir quality (Griffiths et al., 2019) but this approach is not routine. Understanding the relative influences sea level, tectonics, sediment supply and climate, together with depositional processes and subsequent diagenetic controls will lead to improved reservoir quality interpretations which in turn will enhance the prediction of reservoir quality away from, and between, well control points.

Here, we have investigated the influence of depositional processes on the reservoir quality of shallow-buried siliciclastic reservoir rocks in the Weald Basin. The current burial depth is less than 1000 metres, but burial restoration by Palci et al. (2018) has the Upper Jurassic buried as deep as 1500 m in the northern flank of the Weald Basin, before uplift to current depths. These Upper Jurassic rocks in the Weald Basin are dominated by eogenetic processes as they have not been buried very deeply, so that the physical and chemical processes that result from mesodiagenesis, and typically obscure depositional and eogenetic signals, have not occurred. This study focuses on sandstones from the Upper Jurassic Corallian Group (Fig. 2C), which were deposited during a period of active tectonism and sea level rise. The Corallian Group is dominated by carbonate lithologies across much of the UK (Arkell, 1933) but there are Corallian sandstones at outcrop on the Dorset coast (Allen and Underhill, 1989; Goldring et al., 1998) and in Calne, Wiltshire (de Wet, 1987). The Corallian sandstones are locally-important oil-bearing rocks in the Weald Basin (Trueman, 2003). We aimed to understand the relative contributions of eustasy, tectonism and climate on sediment supply and deposition in this shallow marine depositional environment with the aim of appreciating their relative impacts on reservoir quality. The two oil fields employed in this study, Palmers Wood and Bletchingley, are relatively close to London and other populous parts of the SE of the UK. Given the proximity of these oil fields to energy-hungry areas and the UK's progressive drive to carbon-neutrality, it is possible that these relatively old petroleum discoveries could be re-purposed, in the near future, for one or other of carbon capture and storage, compressed air storage or hydrogen storage. Understanding the sedimentology, internal architecture and distribution of reservoir quality of Corallian sandstones may become increasingly important as the energy transition advances. This study addressed the following questions:

1. What were the tectonic, eustatic and climate conditions prevalent during the deposition of the Corallian sandstones in the Weald Basin?
2. What were the consequences of syn-sedimentary tectonism on reservoir architecture and reservoir properties (especially porosity)?
3. What controls reservoir quality in the Corallian sandstones in the Weald Basin?

To answer these questions, we have analysed primary and secondary sedimentary structures in core, defined depositional facies and looked for links between sedimentological expressions and reservoir quality. We also looked for relationships between wireline log data, sedimentology and reservoir quality.

2. The Weald Basin

2.1 Background geology and tectonism

The outcrop geology of the Weald Basin reveals much about its tectonic history (Fig. 1). The Weald Basin is bound to the north by the London-Brabant platform, to the south by the Portsdown-Paris Plage ridge (Portsdown-Middleton trend), the Hampshire and Wessex Basins to the west and it merges into the Paris Basin to the east (Butler and Pullan, 1990; Hansen et al., 2002) (Fig.1). The basement of the Weald Basin includes extensively-deformed later Palaeozoic (Middle Devonian to Lower Carboniferous) rocks whose deformation occurred during the Hercynian orogeny (Butler and Pullan, 1990; Taylor et al., 2001) (Figs. 1B and 2A). The Hercynian deformation event was characterised by north-south compressional forces with resultant east-west thrusts (Fig. 1B) in the basement rocks (Butler and Pullan, 1990; Hansen et al., 2002; Trueman, 2003).

The Weald Basin formed as a result of thermal subsidence after late Triassic to early Jurassic extensional faulting (Lake and Karner, 1987), when north-south crustal extension, utilising earlier Hercynian east-west faults, caused the Weald area to subside south of the stable London-Brabant Platform (Hansen et al., 2002; Trueman, 2003). Sherwood Sandstone Group sediments, important geothermal and petroleum reservoirs in the Wessex Basin to the west (Downing et al., 1983; Hogg et al., 1996), do not typically extend into the Weald Basin as Mesozoic sedimentation in the Weald generally commenced with Rhaetian-Hettangian transgression over Devonian and Carboniferous basement (Andrews, 2014).

The Lower Jurassic saw the deposition of the transgressive limestone-shale units of the Lower Lias over the Palaeozoic basement which was followed by Middle Lias shale and Upper Lias shale-sandstone units (Andrews, 2014; Sellwood et al., 1986). The presence of sandstones in the Upper Lias has been attributed to regression by Sellwood et al. (1986). Extensive carbonate ramp structures in the Middle Jurassic led to the deposition of the Inferior Oolite and the oil-bearing Great Oolite Formations (Butler and Pullan, 1990; Heasley et al., 2000) whose passage into quieter conditions are marked by the muddy and ferruginous units towards the centre of the Weald Basin (Sellwood et al., 1986). Isopach maps from Sellwood et al. (1986) show the deposition of the upward-coarsening, intensely-bioturbated transition muddy sandstones of the Kellaways Beds with clays at the base and sand at the top (Ebukanson, 1984).

Through the Upper Jurassic to Lower Cretaceous, the Weald Basin became a significant depocentre during continued thermal subsidence, with associated active faulting and deposition of the basinal, black, and commonly laminated Oxford Clay Formation (Butler and Pullan, 1990; Hansen et al., 2002; Sellwood et al., 1986) (Fig.1). The Oxford Clay Formation was followed by the deposition of the shallow marine Corallian Group (Fig. 2C), the subject of this study, in the Upper Jurassic Oxfordian stage, during a period of marine transgression and tectonic activity (Sellwood et al., 1986; Sun, 1992). Sun (1992) placed Corallian sandstones, at the top of the Corallian Group, in the Early Kimmeridgian, which was a period of marine transgression (Fig. 2B and 2C). Deposition of the Corallian Group was also a time of the development of extensional east-west, low angle faults (Hansen et al., 2002; Hawkes et al., 1998) that now separate Palmers Wood and Bletchingley oil fields. The Corallian Group was followed by marine deepening and deposition of the Kimmeridge Clay Formation (Hallam, 1978) during a period of sea level rise and increased seismicity, with evidence indicating contemporaneous fault activity during the deposition of the Kimmeridge clay (Fig. 2).

Deposition of the bioturbated, glauconitic Portland sands, during the Tithonian, marks the uppermost Jurassic unit (Andrews, 2014) which was sourced from the London-Brabant massif to the north (Hawkes et al., 1998). The Portlandian was succeeded by a relative sea-level fall, during hot arid conditions, and the consequent deposition of sabkha-type, anhydrite-bearing lower Purbeck sediments (Upper Portlandian to Ryazanian) signalling a regressive episode (Andrews, 2014; Butler and Pullan, 1990; Hansen et al., 2002). The Wealden clay then succeeded the Ryazanian Purbeck group during the Lower Cretaceous Valanginian stage (Andrews, 2014). Sellwood et al. (1986) interpreted the zero isopachyte for the Weald as result of erosion from Cimmerian tectonic activity (Fig. 2) and lowstand sea level.

The overlying thin Gault-Upper Greensand succession has been interpreted to signal the gradual cessation of fault movements and transgression (Butler and Pullan, 1990) or post-Cretaceous erosion (Sellwood et al., 1986). Although well-exposed along the south and north margins of the Weald Basin (i.e., the South and North Downs), the overlying Chalk Group is absent, or too thin for seismic identification, in the Weald Basin (Sellwood et al., 1986); it is not possible to be definitive about seismic activity during its deposition. Chadwick (1985a) suggested that the Chalk Group was deposited during compaction-subsidence of underlying sediments (Butler and Pullan, 1990; Chadwick, 1985b).

The Cenozoic was a period of fault reactivation and uplift in the Weald Basin, including Palmers Wood and Bletchingley oil fields, due to regional-scale compressional movements (Hawkes et al., 1998; Hillis et al., 2008). The uplift has been attributed to two factors, the opening of the North Atlantic which led to regional uplift in the Paleogene and a second phase in the Miocene associated with the Alpine tectonism (Jones, 1999) or possibly the Pyrenean Orogeny (Parrish et al., 2018). Cenozoic inversion was discussed by Hillis et al. (2008); in the Weald, it manifested as a large scale N-S anticline. Uplift has been estimated to range from as little as 701.4 m (2300 ft), based on mapping and extrapolating a base chalk surface (Chadwick, 1993), to as much as 2276.7 m (7470 ft), based on the analysis of sonic logs compared to normal compaction trends of the Oxford Clay Formation (Law, 1998). The basin inversion and uplift led to the formation of broad, dome-shaped hanging wall anticlines, with subsidence of the London Basin to the north and the linked Hampshire-Weald-Dieppe Basins to the south, during the late Palaeocene-Eocene (Hansen et al., 2002).

2.2 Conditions during the deposition of the Upper Jurassic in the Weald area

The Jurassic was a greenhouse period with no polar ice caps, and tropical and subtropical zones that were wider than present day ranges (Hallam, 1975; Hallam, 1977, 1984; Talbot, 1973). In the Oxfordian, when the Corallian was deposited, the palaeolatitude of Britain is estimated to have been in the subtropical range between 31° N and 37° N (Hallam, 1975) or alternatively about 24°N (Scotese, 2001). The climate was generally warm with peak temperatures in present-day NW Europe (Britain) occurring in the Kimmeridgian (Haq, 2017). However, Ruffell and Rawson (1994) concluded that the aridity/humidity of the local land-masses of southern and eastern England, England, NW Europe and southern France during the deposition of the Corallian (in the Oxfordian) have not been well documented. Nonetheless, a study by Hallam (1984) suggested the occurrence of a humid Jurassic climate in eastern, central and north-western Europe up until the Kimmeridgian.

It has been concluded that Jurassic sea levels were not significantly different to present day sea levels, as suggested by Hallam (1981); Haq (2017); Hardenbol et al. (1998) (Fig. 2B); it was inferred, by these authors, that the Upper Jurassic was a period of overall sea level rise. A modified curve of Upper Jurassic sea levels (Fig. 2B), as documented by Haq (2017), presents a eustatic rise in sea level from the Lower Oxfordian through to the Kimmeridgian, as well as several short-term sea level falls of uncertain magnitude.

3. Datasets and methodology

3.1 Sedimentary logs

This study focused on the examination of Corallian cores from three wells, Palmers Wood-3 (PW3), and -7 (PW7) and Bletchingley-5 (BL5), from the Weald Basin, onshore SE England (see Fig. 1). The cores are held at the British Geological Survey (BGS) core store in Keyworth, Nottinghamshire. The three wells were initially logged at high resolution (1:24). PW3 had 17.1 m of core, PW7 had 16.6 m of core and BL5 had 19.8 m of core. Measured depths from the cores were converted into true vertical depth by taking well deviation into account. The present-day true vertical depths to the top of the Corallian sandstones are BL5: 844.2 m, PW7:875.4 m and PW3: 904.1 m. Each core was logged for lithology, grain size, sedimentary structures, ichnology, bed contacts, cement types and degree of cementation. Ichnofabrics were described using the approach defined by Pemberton et al. (2012). Lithology, grain size and sedimentary structures were recorded to determine primary depositional conditions. Bed contacts and ichnology was recorded to give indications of primary depositional conditions andsequence stratigraphic surfaces such as discontinuities.

Sedimentary logs were summarised and digitised at a resolution of 1:120, with their facies classified based on texture and lithological attributes following Farrell et al. (2012). Facies associations were interpreted to help determine depositional environments, using methods described by Hampson and Storms (2003) and Kamola and Van Wagoner (1995) relevant for shallow marine shoreface to shelf depositional environments.

3.2 Petrography

Petrographic analysis of the Corallian sandstones was carried out using automated Scanning Electron Microscopy-Energy Dispersive Spectroscopy (SEM-EDS) and optical microscopy. Fifty-one polished thin sections (30 μm thickness) were prepared from rock samples from the three cores with samples first injected with blue dyed resin to highlight any porosity. Twenty-three samples were from BL5, nine were from PW3, and 19 were from PW7.

Optical petrography, using an Olympus BX51 transmitted light microscope, was carried out to investigate lithology, micro-textures, cement types and mineralogy. Samples were point counted, using a CVS Petrog stage, for 300 counts per section.

SEM-EDS was undertaken to provide a quantitative evaluation of mineral proportions as well as grain and pore space morphology. The equipment used in this study was an FEI WellSite QEMSCAN, at the University of Liverpool, equipped with a tungsten-filament, operating at 15 kV and two Bruker EDS detectors (Wooldridge et al., 2018). The QEMSCAN is made up of a scanning electron microscope equipped with energy dispersive X-ray spectrometers and is capable of automated mineral identification from an extensive mineral database known as Species Identification Protocols (SIPs) (Armitage et al., 2010; Pirrie et al., 2004). SEM-EDS has spatial resolution of about 1 μm, thus it cannot identify minerals grains or pore space less than 1 μm. Mineral quantification with SEM-EDS is accurate to within fractions of a percent.

3.3 Wireline logs

Gamma ray, neutron porosity, sonic velocity, density and resistivity logs from PW7, PW3 and BL5 were available for analysis. For the overall interpretation of lithology and fluid saturation, porosity was derived from the density log using:

$$\text{Porosity}\ (\phi_{\text{RHOB}}\ \%) = 100\,.\,\frac{\rho_{\text{meas}} - \rho_{\text{b}}}{\rho_{\text{matrix}} - \rho_{\text{fl}}}$$

(Equation 1)

Where ρ_{matrix} is the assumed matrix (rock) density, ρ_{meas} is the reported log (bulk) rock density (ρ_b) and ρ_{fl} is the assumed fluid density for the invaded zone of the near well-bore region.

The fluids in the pore space were divided into water and petroleum using the deep resistivity log (R_d) and equation 2, the Archie equation:

$$S_w = \sqrt[n]{\frac{a\,.\,R_w}{\phi_{\text{RHOB}}^{m}\,.\,R_d}}$$

(Equation 2)

Where S_w is the fractional water saturation, a, m and n are the Archie constants (default values: 1, 2 and 2 but modified here to fit the S_w to as close to 1.00 as possible in the water leg), ϕ_{RHOB} is the porosity determined using the density log (equation 1) and R_d is the deep resistivity of the formation. Formation water salinity was assumed to be between 85,000 and 100,000 ppm, resulting in an in-situ resistivity (R_w) of about 0.06 ohm.m (Trueman, 2003).

The solid part of the rock was split into proportions of shale and sand using gamma log data and the Vshale calculation:

$$\text{Vshale} = \frac{\text{GR}_{\text{meas}} - \text{GR}_{\text{min}}}{\text{GR}_{\text{max}} - \text{GR}_{\text{min}}}$$

(Equation 3)

Where GR_{max} is the maximum gamma value for the reservoir-top-seal section of interest, GR_{meas} is the measured gamma value for the depth of interest and GR_{min} is the minimum gamma value for the reservoir-top-seal section of interest.

The computed wireline lithology and neutron-density cross-over plots were used to define pay and non-pay zones and to help deduce correlations between wells. Gamma ray logs were used for correlations across facies associations to determine the lateral continuity of facies associations between wells and tectonic structures. Core-to-log depth-shifts were applied to allow comparison of core and log data and true vertical depths calculated to put the porosity data into context of the present-day depth of burial and possible extent of uplift.

4. Results

4.1 Sedimentary logs

In the following sections, where we refer to depth in text or on figures, all depths are reported in terms of measured (as opposed to true vertical) depth in metres (m-md) but were originally reported in units of feet. We also have used a single key to represent the logged data from cores (Fig. 3) as shown in Figure 4 for the sedimentary logs in Figures 5, 6 and 7. All cores were dominated by light grey to brown sandstones, siltstone and minor dark brown to black mudstones (Fig. 3). Bivalve clasts are common and appear as white and grey, thin curved shells in core (Fig. 3), especially in the coarser grained sections. Grain size varies from clay, through silt to coarse sand with beds showing repeated coarsening upward cycles. Some of the coarsening upward cycles then reverse into a fining upward cycles (Figs. 5-7).

The Mudstones are predominantly highly bioturbated (Fig. 6, 1096.7-1097.9 m) and mainly occur as thin beds or laminae within the sandstones (Fig. 6, 1089.6 m), or at the boundary with the underlying Corallian argillaceous unit (Fig. 5 at 1138.0 m) and overlying Kimmeridge Clay (Fig. 5 at 1122.5 m). Typical sedimentary structures include lenticular bedding, cross-lamination, mottled fabrics where bioturbation has obscured primary depositional features, and massive featureless beds that may be wholly bioturbated. Mudstones in core are apparently free of bioclasts (Fig. 3E).

The Siltstones are present adjacent to mudstones at the upper boundary of the Corallian argillaceous unit and the lower boundary of the Kimmeridge Clay, and in the middle section of PW7 (Figs. 5, 6, 7). Sedimentary structures in the siltstones include lenticular bedding (BL5 at 2193.6 m), mud drapes, mottled fabric (PW7 at 1128.9 -1129.6 m) and massive bedding (PW3 at 1081.4 m).

Sandstones make up most of the Corallian section with a range of sedimentary structures including: planar-, trough- and hummocky-cross-bedding, massive-bedding, lenticular- and flaser-bedding, as well as current-, wave- and climbing-current ripple lamination (Figs. 5, 6 and 7). Bed types seem to be randomly stacked over short vertical intervals (Figs. 3C, 5, 6 and 7). Bivalve clasts are common and appear as white and grey pin-shaped, curved shells in core (Fig. 3), especially in the coarser grained sections.

Secondary features in the Corallian sandstones include cementation, bioturbation, erosional surfaces and hydrocarbon staining. The cores have variable degrees of carbonate cementation as well as hydrocarbon staining (Fig. 3), with dark brown hydrocarbon staining found in the poorly cemented, more porous zones (Fig. 3B) and negligible hydrocarbon staining in highly cemented zones (Figs. 3A and 3C). Bioturbation is common but with varying intensity and diversity. Intense bioturbation has resulted in a mottled fabric (Fig. 3C) as well as mixing clean sands beds with more clay-rich beds (PW3, 1087.5-1089.4 m). Bioturbation intensity is here described on a scale of 0-6 using the Taylor and Goldring (1993) index. Common ichnofabrics include Skolithos ichnofacies (Seilacher, 1967) with *Skolithos, Ophiomorpha* and *Diplocraterion* (Fig. 3, 5, 6 and 7); the Cruziana ichnofacies (Seilacher, 1967) with *Rhizocorallium*, *Rosellia, Teichichnus, Thalasinoides* as well as Zoophycos ichnofacies (Pemberton et al., 2012) with *Chondrites* (Fig. 3D and 3E). Some non-graded bed boundaries were erosive with sharp changes in grain size locally accompanied by abrupt increases or decreases in the degree of bioturbation (Fig. 5, 6 and 7).

4.2 Interpretation of sedimentary logs

The localised variations of grain size and sedimentary structures in the Corallian sandstones in the three wells (Figs. 5, 6 and 7) indicates variable energy conditions during deposition. Abrupt decreases in grain size can be interpreted in different ways. For example, reductions in grain size in PW7 (at 1122.8 m), PW3 (at 1082.0 m) and BL5 (at 2193.9 m) are here interpreted as flooding surfaces as they are succeeded by a change in lithology to shale, signifying an increase in water depth (Walker and James, 1992) while changes in grain size above scours (e.g. Fig. 3D) represent erosional surfaces which have here been interpreted as erosional or non-depositional (hiatal) discontinuities (Hampson and Storms, 2003) (Figs. 5, 6 and 7).

Based on grain size and both primary (bed-relationships) and secondary (bioturbation) sedimentary structures, a total of 12 facies have been identified (Table 1). The ichnofacies in the Corallian sandstones indicates varied energy conditions during deposition. *Skolithos, Ophiomorpha* and *Diplocraterion* of the Skolithos ichnofacies are typical of episodic high energy erosion and sedimentation events (Seilacher, 1967) while the Cruziana and Zoophycos ichnofacies are typical of deposition under lower energy conditions (Pemberton et al., 2012; Seilacher, 1967). The occurrence of both the Skolithos and Cruziana ichnofacies re-emphasises the varied energy conditions during the deposition of these sandstones. The diversity of the facies suggests varied hydrodynamic conditions during marine deposition. For example, the massive mudstone facies (Mm) was deposited from suspension under low-energy, sediment-starved conditions (Walker and Plint, 1992) with a slow rate of deposition under quiescent conditions conducive for sediments to be reworked by fauna (Gowland, 1996). Sandstone facies represent deposition in relatively high energy conditions; for example, planar cross-bedded sandstones, trough cross-bedded sandstones and low angle cross-bedded sandstones of the cross-bedded sandstone facies (Sx) are products of dune migration under high energy condition (Vakarelov et al., 2012) and hummocky cross-bedded sandstone represent deposition by storm events (Pemberton et al., 2012; Vakarelov et al., 2012).

From a reservoir quality perspective, the dominance of sand in this part of the Corallian is an indicator of potential reservoir zones. Although there is no simple relationship between cementation and depositional facies, the occurrence of hydrocarbon staining only in the less-cemented intervals indicates that porosity has been destroyed by cementation (Fig. 3A and 3B). Reservoir presence has also been affected by homogenisation of sand and clay beds and laminae by bioturbation which has locally reduced the net clean sand fraction in some bioturbated sections of core (Fig. 3C and 3D).

4.3 Wireline logs

The wireline logs were converted to fractions of sand, shale, water and oil using equations 1, 2 and 3 (Figs. 5B, 6B, 7B). The interpreted lithology logs reveal sand- and shale-rich sections in the Corallian, including relatively coarse beds that contain abundant clay minerals due to bioturbation (Fig. 6 at 1088.9 m). The interpreted lithology logs have good relationships with the neutron density cross-over logs, delineating sections with potentially good reservoir. The neutron-density cross-over plots together with the lithology logs reveal the dominantly sand-rich lithology of the Corallian sandstones evolving from the underlying shale-rich Corallian argillaceous unit and into the overlying shale-rich Kimmeridge Clay (Figs. 5B, 5C, 6B, 6C, 7B, 7C). All three wells show a decrease in sand- and increase in shale in the middle of the Corallian section, representing an intra-Corallian shale horizon. In addition, BL5 also has an extra clay-rich section at 2199.0 -2201.5 m.

The wireline-derived lithology, the neutron-density cross-over plots and the gamma ray logs show the intra-Corallian argillaceous section correlates across all three wells (Figs. 8 and 9). The two deepest sandstone packages (S1 and S2) seem to correlate from PW3 and PW7 to BL5. However, by reference to the true vertical depths, there is a distinct thickening (of more than 4.27 m) of the Corallian sandstones southward from Palmers Wood to Bletchingley (Fig. 8). The sandstone package at the top of BL5 (labelled S3 in Fig. 8) does not correlate with any of the sandstone packages in the Palmers Wood wells and accounts for the southward thickening of the whole Corallian sandstones (Fig. 9).

The correlated sandstones, above and below the intra-Corallian mudstone, all show variable, but locally fair to good, porosity (Figs. 5, 8); in contrast, the top-most sandstone in BL5 seems to be different, having uniformly low porosity (Figs. 7 and 8).

BL5*4.4 Petrographic data*

Optical microscopy and SEM-EDS data help support interpretation of the conditions during deposition; they reveal that the Corallian is locally quartz-rich with minor feldspars, berthierine-ooids, phosphate ooids, bioclasts and minor clay-rich lithic grains (Figs. 10A, C and 11A). Sandstone grain sizes range from coarse- and medium- (Figs. 10A and C) to fine-grained (Figs. 12A and B). The cements include calcite, dolomite, siderite, pyrite, berthierine, quartz and kaolinite (Figs. 10, 11 and 12). There is no evidence for the development of evaporitic cements, such as gypsum.

Pore-filling detrital clay minerals are composed of illite, berthierine and kaolinite (Fig. 12). Other poor-filling, fine-grained minerals include biotite, K-feldspar, plagioclase feldspar and rutile (Fig. 12).

Petrographic images reveal a relatively uncompacted texture where grains are separated from each other by cement or pore spaces (Figs. 10 and 11). In cases where the detrital grains are in contact, they dominantly have face-to-edge contacts (Fig. 10C). Sandstones range from coarse- and medium- (Figs. 10A and C) to fine-grained (Figs. 11A and C). Disarticulated bivalve clasts are most common in the coarsest grained fractions (Fig. 10A and C). Acicular cement occurs around bivalve fragments, suggesting marine cementation (Scholle and Ulmer-Scholle, 2003) (Figs. 10 A, C). Bioclasts show a great degree of micritisation of their edges (Adams, 1998; Tucker, 1981), even in completely neomorphosed bioclast grains (Fig. 10), confirming that the Corallian was deposited in the marine photic zone.

Modal analysis (point count) data are shown in a ternary plot (McBride, 1963), in Figure 12C with Q representing the sum of polycrystalline and monocrystalline quartz. F is the sum of plagioclase and K-feldspars and L is the sum of all lithic fragments including extrabasinal mudstone, extrabasinal chert, extrabasinal sandstone, extrabasinal quartzite, muscovite, berthierine and bioclasts. The ternary plot shows a composition typical of a quartz arenite, with minor subarkoses and sublitharenites (Fig. 12C). The plots show no distinct distribution of QFL by facies association except for the offshore facies association, which has slightly elevated feldspars and the upper shoreface which shows a high lithic content. The distribution of feldspars in the offshore facies association is due to the abundance of fine-grained feldspars in the lower energy, argillaceous zones (Figs. 11B and 12B). Lithic fragments are abundant in the upper shoreface facies association because the high density larger bioclasts and ooids can settle under high energy upper shoreface environments.

SEM analysis revealed that calcite is the main cement, with an average of up to 39% (Fig. 13B). Dominant calcite cement can be seen in images where the SEM image is next to an equivalent optical image, e.g., Figs. 10, 11A and 11B as well as 12A and 12B with abundant calcite cement evident in samples with elevated bioclast concentrations (Figs. 10 and 11C) and less abundant in samples with fewer bioclasts and clay minerals (Figs. 11A and 12). This relationship is also seen at the well-scale where BL5 has fewer bioclasts and clay minerals and more calcite (Fig. 13B, 13C and 13D). The dominant calcite cement fills pore spaces and separates framework grains from each other, suggesting an early origin (Fig. 10). Longitudinal grain contacts are not common in these sandstones as early calcite cementation has filled pores and hindered pore-loss due to compaction (Fig. 10A, 10B, 10C and 10D). Calcite-poor samples have higher porosity (Fig. 11A and 13). It is also worth noting that bioclasts are less abundant in finer-grained, clay-rich samples (Fig.11C) and more abundant in the coarse-grained, clay-poor samples (Fig. 10). The relationships between bioclasts, grain-size and clay content suggests a hydrodynamic control on bioclast accumulation.

4.5 Facies associations and depositional environments

Five facies associations (Table 2) were derived from the 12 facies (Table 1) to help reveal the overall sedimentary environment of these relatively thin bedded, variably bioturbated and complex sediments. These facies associations include foreshore, upper shore face, proximal lower shoreface, distal lower shoreface and offshore shelf/ramp facies associations (Table 2). The facies associations are presented below in order of decreasing energy conditions.

4.5.1 Foreshore facies association (FSFA)

The foreshore facies association (Table 2) is composed of fine- to medium-grained, low angle, planar-parallel laminated sandstones (Fig. 3A). The foreshore facies association is absent in PW7 (Fig. 9) but forms thin beds in PW3 and BL5, with the thickest beds in the lower sandstone unit of PW3. The foreshore facies association has a sharp basal contact with the upper shoreface facies association in PW3 (Fig. 6A at 1085.1 m). The foreshore facies association is commonly non-bioturbated, but where, bioturbated it displays low intensity *Macaronichnus* (Fig. 6A at 1090.0 -1091.8 m).

Foreshore facies association sandstones are well-sorted to very well-sorted with sub-rounded to rounded grains (Fig. 10A). They show an abundance of disarticulated bivalve shells aligned in one direction suggesting transport of the bioclasts into and within the depositional environment (Fig. 10A). The coarser-grain sizes, disarticulated bivalve shells, rare bioturbation and sharp contacts with other facies associations suggest high energy deposition of this facies association similar to lithofacies unit 3 of Sun (1992), who described deposition in a shallow, high energy environment. These sandstones are, however, not glauconitic as described in Sun (1992); instead they contain the Fe-clay mineral berthierine. It seems that Sun (1992) mistook berthierine for glauconite as both are green marine clay minerals.

4.5.2 Upper Shoreface facies association (USFA)

The upper shoreface facies association (Table 2) is the most common facies association in the three wells; it is characterised by upper fine- to medium-grained sandstone. Massive, structureless bedding is common (Fig. 3B) as well as trough cross-bedding (Fig. 6A), planar cross-bedding (Fig. 6A) and localised low angle cross-bedding (Fig. 5A). Minor planar lamination (Fig. 5A) and hummocky cross-stratification (Fig. 5A) and wave ripple lamination (Fig. 7, 2210.9 m) are also present.

Sandstone body thicknesses are variable, from less than thirty centimetres (Fig. 6A, 1092.5 m) to greater than four metres (Fig. 5A, 1129.6 -1135.8 m). Some beds within individual sand bodies display upper and lower erosive contacts within the upper shoreface facies association (e.g., Fig. 5A at 1134.8 m) indicating high energy conditions.

Ethological expressions are sparse to moderate probably because of high energy depositional conditions. Where present they include: *Ophiomorpha, Skolithos, Planolites, Cylindrichnus, Anchonichnus* and *Macaronichnus* (Figs. 5-7) supporting an interpretation of high energy deposition.

Erosive lower contacts occur between the relatively high energy, upper shoreface facies association sediment and underlying lower energy facies associations, e.g., on proximal lower shoreface facies association (Fig. 5A at 1135.9 m; Fig. 7A at 2211.1 m) and on distal lower shoreface (Fig. 6A at 1087.5 m). These erosive contacts reveal sudden, rather than gradational, increases in energy conditions.

Sharp upper contacts are common between the high energy, upper shoreface facies association sediment and overlying finer-grained, lower energy facies associations, e.g., with offshore facies association and with distal lower shoreface facies association (Fig. 5A at 1129.6 m). These sharp contacts also represent a sudden, as opposed to gradational, change in energy conditions.

In contrast, gradational upper contacts occur between the high energy, upper shoreface facies association sediment and overlying high energy foreshore facies association (Fig. 7A at 2203.6 m).

Carbonate cementation, visible in core in the upper shoreface facies association, is variable and is broadly proportional to the quantity of micritised, detrital, disarticulated bivalve shells (Fig. 10C). The pronounced preferential alignment of bivalve shells (Fig. 10C) suggests deposition following high energy current transport.

Upper shoreface facies association sediments are interpreted as deposits above fair wave base under the influence of wave activity. The low degree of bioturbation (Figs. 3B, 5-7) implies high energy conditions which were intermittently interrupted by the low energy conditions, in the photic zone, as evidenced by the alignment of micritised bivalve shells (Pemberton et al., 2012; Salah et al., 2016). The erosively-amalgamated beds within sand bodies occur due to stacking that indicates continuous deposition succeeding erosion, rather than completely eroded older beds (Hampson and Storms, 2003). This facies association is similar to lithofacies 3 and 5 of Sun (1992), with medium-grained trough cross-bedded, planar cross-bedded, structureless-bedded and low angle cross-bedded sandstones with many shell fragments typical of high energy depositional environments.

4.5.3 Proximal Lower Shoreface facies association (pLSFA)

The proximal lower shoreface facies association (Table 2) is characterised by upper fine- to fine-grained amalgamated sandstone beds (Fig. 7, 2211.1 -2212.8 m). Proximal lower shoreface beds commonly have current ripple lamination (Fig. 6, 1095.1 m), cross lamination (Fig. 7, 2211.6 m) and mud-drapes (Fig. 5, 1128.2 m). These sediments are moderately- to intensely-bioturbated with common ichnofossils in argillaceous zones including *Anconichnus, Ophiomorpha, Palaeophycus, Rhizocorallium, Cyclindrichnus, Teichichnus rectus, Thalasinoides* and *Chondrites* (Fig. 3C). Bed thicknesses vary from less than centimetre-scale laminae (Fig.7 at2206.1 m) to beds that are about 2.13 m thick (Fig.5A at1137.5 m). Beds in this facies association commonly have erosive lower contacts with distal lower shoreface facies association sediment (Fig. 5A at1128.4 m and 1138.2 m). Carbonate cementation is variable; it seems to be most intense in the most highly bioturbated zones (Fig. 3C and Fig. 5A at 1137.6 m).

Based on grain size, sedimentary structures and degree and type of bioturbation, the proximal lowershoreface sandstones are interpreted to have been deposited under moderate energy conditions when the influence of wave action above the storm wave base was dominant (Pemberton et al., 2012). The moderate- to intense-bioturbation suggests that periods of low deposition rate and non-deposition were more prevalent in these proximal shoreface sandstones than in upper shoreface sandstones. The occurrence of bed amalgamation suggests repeated high energy conditions that interrupted ambient moderate energy conditions (Vakarelov et al., 2012), mostly likely due to storm activity (Hampson and Storms, 2003).

4.5.4 Distal Lower Shoreface facies association (dLSFA)

Siltstones and fine-grained sandstones are the dominant lithology in the distal lower shoreface facies association (Table 2), which also hosts minor medium grained sandstone (Fig. 3D). These sandstones are moderately-sorted to poorly-sorted mostly due to their high clay content and are composed of sub-angular to sub-rounded grains (Fig. 11C and D). Sedimentary structures include hummocky cross-stratification, minor wavy lamination and wave ripple lamination (Figs. 5-7). Beds are mainly non-amalgamated (Fig. 3B). These distal lower shoreface sediments show moderate to intense bioturbation, suggesting deposition in low energy conditions with low input of sand-grade sediment but in aerobic and nutrient-rich conditions (Seilacher, 1967). Erosive amalgamation of non-bioturbated, distal lower shoreface beds is relatively rare (e.g., Fig. 6A at 1088.1 m).

Distal lower shoreface sandstones are mostly thin-bedded, typically varying from less than ten centimetres to half a metre (Fig. 6A at 1095.6 m) but reaching up to about two metres (Fig. 6A). These sandstones are commonly erosively overlain by higher energy facies associations, e.g., proximal lower shoreface (Fig. 5A at 1128.4 m) and upper shoreface facies associations (Fig. 6A at 1087.5 m).

Ethological expressions in distal lower shoreface sandstones are dominated by the Cruziana ichnofacies and include *Anchonichnus, Chondrites, Ophiomorpha, Planolites, Palaeophycus, Rosellia, Rhizocorallium, Terebellina*, *Teichichnus rectus* and *Thalasinoides* (Fig. 3D, Figs. 5 to 7). The presence of Cruziana ichnofacies suggests intensive deposit feeding behaviour typical of low energy environments (Pemberton et al., 2012). These sandstones are similar to lithofacies 2 of Sun (1992) and composed of very fine to fine-grained intensely bioturbated sand deposited under fluctuating storm activity. The distal lower shoreface facies association is here interpreted to have been deposited below storm wave base, with deposition mostly from suspension, probably between storm events (Hampson and Storms, 2003; Pemberton et al., 2012). The non-amalgamated beds typify low energy deposition from low velocity flow connoting a predominance of low energy regimes with little significant erosion (Vakarelov et al., 2012). Localised erosively-amalgamated non-bioturbated beds suggest high energy pulses from storm-induced higher energy conditions capable of injecting coarser grains and eroding bed boundaries (Andrieu et al., 2016; Hampson and Storms, 2003).

4.5.5 Offshore Shelf/Ramp facies association (OSFA)

This facies association is composed of dark mudstone, siltstone, and some thin beds of fine-grained sandstone (Fig. 3D; Table 2). The main sedimentary structures include wave ripple lamination, current ripple lamination and heterolithic bedding (Figs. 6 and 7). Lenticular bedding is present but rare in this facies association.

Bioturbation tends to be intense and there is wide diversity of ichnofabrics with ichnofossils mostly belonging to the Cruziana ichnofacies. These include *Chondrites, Cylindrichnus, Planolites, Palaeophycus, Terebellina, Teichichnus zigzag, Teichichnus rectus, Thalasinoides* and *Rhizocorallium*.

The offshore shelf/ramp facies association shows a sharp basal contact with the upper shoreface at the top of PW7 (Fig. 5); this represents an erosive basal contact with the upper shoreface in the intra-Corallian section, at 1129.6 m. In PW3, the basal contact of the offshore shelf/ramp facies association is erosive (Fig. 6A at 1082.2 m) and is interpreted as a flooding surface.

The offshore shelf/ramp facies association is interpreted to have been deposited below storm wave base, mostly from suspension in low energy water as evident by occurrence of siltstone and mudstone as well as the abundance of the Cruziana ichnofacies (Pemberton et al., 2012).

The offshore shelf/ramp facies association is found mostly in the upper and lower part of the Corallian section (Figs. 5, 6 and 7). Only PW3 contains about half a metre of this facies association in the middle section (Fig. 5). The offshore shelf/ramp facies association at the bottom and top boundaries of the Corallian sandstones represent transition from the Corallian argillaceous section and to the Kimmeridge Clay, respectively. This facies association is similar to lithofacies unit 1 of Sun (1992), as it is diagnostic of low energy deposition of mostly fine-grained sediments with sedimentary structures, such as ripple lamination and low energy ichnofabrics such as chondrite.

4.6 Breaks in sedimentation

4.6.1 Erosional discontinuities

Erosional discontinuities are common throughout the Corallian sandstones. Erosional surfaces may indicate a lowering of storm wave base due to minor fall in sea level or due to storm events (Hampson and Storms, 2003). The presence of erosional discontinuities here have been interpreted where there is an increase in grain size and a reduction in bioturbation intensity in beds overlying an erosional bed contact (Fig. 5A at 1126.1 m and 1128.4 m, 1134.8 m, 1137.1 m, 1137.6 m and Fig. 6A at 1088.1 m).

Inferred erosional discontinuities (represented by dotted lines on Figs. 5, 6 and 7) have been added where there is either (i) a sharp increase in grain size (but no change in bioturbation) or (ii) a marked decrease in bioturbation intensity (but no increase in grain size). Erosional contacts are common in the high energy, wave-dominated facies associations, e.g., in the upper shoreface facies association in BL5 (Fig. 7A), in the proximal lower shoreface facies association in PW7 (Fig. 5A) and at the boundary between the distal lower shoreface and the proximal lower shoreface also in PW7 (Fig. 5A).

Correlation of erosional discontinuities is represented in Figure 9 with PW7 and PW3 having three correlations: two at the base of the Corallian and one at the middle (Fig. 9). These correlated discontinuities are at facies boundaries and represent shore-ward shift to higher energy facies associations. Erosional discontinuities are typically succeeded by high energy, storm-related deposits (Fig. 5 at 1137.6-1138.1 m).

4.6.2 Non-depositional discontinuities

The Corallian sandstones have abundant evidence of non-depositional discontinuities. Non-depositional discontinuities are here recognised by a sharp reduction in grain size, an abrupt increase in bioturbation intensity and anomalous (non-contiguous) successions of facies associations (Hampson and Storms, 2003). Non-depositional discontinuities are common in the proximal lower shoreface and upper shoreface facies associations in BL5 and PW7 and are found in the distal lower shoreface and upper shoreface associations in PW3.

The non-depositional discontinuities are here interpreted to be a result of a drop in energy due to sea-level rise, a tectonically-induced break in sediment supply or waning storm-wave conditions (Hampson and Storms, 2003).

Except for the flooding surface marking the transition to the Kimmeridge Clay Formation at the top of all three wells, only one other non-depositional discontinuity correlated in the middle section of PW7 and PW3 (Fig. 9). The correlated non-depositional discontinuity is at the boundary between the upper shoreface facies association offshore facies association (PW7) and distal lower shoreface (PW3). The correlated non-depositional surface marks a basinal shift to lower energy facies associations in the middle of the Corallian sandstones.

5. Discussion

5.1 Relationship between wireline and sedimentary logs

The variations in the relative abundance of sand and shale proportions in the wireline lithology logs and neutron-density cross-over plot show changes in sand and shale sediment deposition as seen when compared with the sedimentary logs in figures 5,6 and 7. The sedimentary logs show thick sand bodies in all the wells. High gamma ray values are observed in some thick sand bodies due to small-scale, clay-rich sedimentary structures, such as flaser beds, lenticular beds (Fig. 7 at 2206.5 m; Fig. 6at 1088.0 m), mud drapes (Fig. 7 at 2210.4m) and intense homogenisation of sand and clay by bioturbation (Fig. 7 at 2207.4-2208.0m; Fig. 6 at 1088.7 m).

The evolution from deposition of the Corallian argillaceous section to deposition of the overlying Corallian sandstones is represented by the elevated sand fraction, shown by the lithology log and the basal sand in the neutron-density cross-over plot (Fig. 8). Similarly, the top of the Corallian grades into the Kimmeridge Clay Formation where there is a marked decrease in the sand fraction also shown by the lithology log and neutron-density cross-over plots (Fig. 8).

The intra-Corallian mudstone, correlated across this part of the basin, may be the result of a transient increase in sea level (Newell, 2000) that exceeded the rate of supply of sand. Considering that the sandstones were deposited during a period of eustatic sea level rise (Fig. 2), the deposition of clastic sediment indicates that supply of material outpaced sea level rise (Conybeare, 2013). Conversely, the intra-Corallian mudstone and siltstone represents subdued coarse clastic deposition where sea level rise has caused an increase in accommodation space and sediment starvation (Newell, 2000)

The deposition of the upper and lower Corallian sandstones during a period of sea level rise, makes it similar to the highstand deposition interpreted for the Corallian in the Wessex Basin (Newell, 2000). Thus, we have also used a highstand systems tract interpretation for these sandstones.

The sedimentary logs, wireline lithology logs and neutron-density cross-over plots (Figs. 5, 6 and 7) all show agreement in a dominant sand-rich lithology with reservoir potential (pay zones). The correlation of the intra-Corallian section across all three wells splits the reservoir in the Corallian sandstones into an upper and lower unit (Fig.8). The pay zones S1 and S2 have lateral continuity across the three wells (Fig.8) and hence can be predicted away from the wells.

5.2 Correlation of Corallian sandstones and intra-Corallian mudstone

Mudstone packages that correlate across all three wells, M1 (Corallian argillaceous section), M2 (intra-Corallian section) and M3 (base of Kimmeridge shale), mark genetically related lithologic units. Similarly, the sandstone package, S1 below the intra-Corallian section and S2 above the intra-Corallian, also correlate across all three well (Fig.8). The mudstone packages indicate a transient regional reduction in clastic input while the sand packages indicate a regional flux of clastic sediment (Conybeare, 2013; Walker and Plint, 1992).

Mudstone package M* and S3 in BL5 do not seem to correlate with any of the sandstone and mudstone packages in Palmers Wood indicating a local control on deposition. In addition, the Corallian section from S1 to S2 does not show significant thickness variation but the increase in thickness in excess of 4.3 m in M* and S3 is typical of fault-controlled deposition (Childs et al., 2003; de Wet, 1998; Newell, 2000).

Facies associations correlate relatively well between PW7, PW3 and the lower to middle section of BL5 (Fig.9). The upper section of BL5 show non-contiguous juxtaposition of lower energy proximal and distal lower shoreface facies association with upper shoreface facies association. These facies associations at the upper section BL5, which do not correlate with PW7 and PW3, show anomalous juxtaposition typical of syn-depositional fault control (Cecil, 2013; de Wet, 1998).

5.3 Eustatic controls on sediment supply and deposition

Marine deposition of the Corallian sandstones can be inferred from the marine deposition of both the underlying Oxford Clay and overlying Kimmeridge Clay Formations, which were both deposited during periods of sea level rise (Hallam, 1981; Haq, 2017; Hardenbol et al., 1998) and the absence of any evidence of significant regression preceding deposition of the Corallian sandstones. Direct evidence of marine deposition of the Corallian includes eogenetic carbonate and phosphate cements (Fig. 12B), acicular calcite cement fabrics lining bivalves and framework grains (Scholle and Ulmer-Scholle, 2003) (Fig. 10C), presence of marine ichnofossils (Fig. 3), micritisation of bivalve shells (Figs. 10) and the absence of evidence of rhizocretions, paleosols or other signs of emergence surfaces within the Corallian sandstones.

The intra-Corallian mud- and silt-stone, high gamma interval represents a regionally correlated transgressive event (Figs. 8 and 9). The non-depositional surface identified in core at the base of the intra-Corallian section (Figs. 5 to 7) suggests that there was a reduction in energy and sediment supply due to sea level rise outpacing sediment supply. Coarse-grained, high-energy facies associations overlay the intra-Corallian (Fig. 9) suggesting resumption of sediment supply rate outpacing sea level rise. Analysing the lateral extent of the non-reservoir intra-Corallian and reservoir sandstone packages, beyond the case study location, is limited by the number of wells in this study. However, the intra-Corallian section was previously described as lithofacies unit 4 by Sun (1992) and correlated across PW3, PW5, BL2 and Collendean Farm 1 in the Weald Basin. Similarly, in the Wessex Basin, transgressive events were also noted at the equivalent Oxfordian-Kimmeridgian boundary in the nearby Wessex Basin by Sun (1989). The occurrence of the transgressive events in both the Weald and Wessex Basins suggests an allocyclic influence where sea level rise outpaced sediment supply.

Local conditions influenced deposition. Although non-depositional discontinuities (hiatuses) could mark reduction in marine circulation caused by sea level rise, their frequency and lack of correlation across the three wells suggests localised effects (Fig. 9). Similarly, erosional surfaces that do not correlate between wells also suggest local conditions rather than a basin-scale influence expected of sea level rise.

Overall, we can infer that eustasy led to the deposition of the intra-Corallian mudstones but played a muted role in controlling deposition of the Corallian sandstones.

5.4 Tectonic controls on sediment supply and deposition

Although deposited during a period of transgression, the Corallian consists of coarse-grained siliciclastics with several coarsening upward cycles (Figs. 5 to7). These cycles observed in core, confirm coarsening upward cycles reported from gamma ray logs by Sun (1992). This pattern can only be explained by the net rate of sediment supply exceeding the net creation of accommodation space.

Tectonic activity is capable of increasing the rate of creation of accommodation space and sediment supply such that sedimentary expressions typical of transgression are in one part of a basin and regression in other parts of a basin as a result of the interplay of locally variable subsidence and deposition rates (de Wet, 1998; Lake and Karner, 1987; Newell, 2000).

Evidence supporting syn-tectonic depositional controls on the Corallian sandstones include thickening of the Corallian section at the upper section of BL5 in excess of 4.3 m, across the fault separating the Palmers Wood wells from BL5 (Figs. 8, 9 and 14). The position of extra sand and mud packages in the upper section of BL5 suggests that syn-depositional faulting occurred in the final stages of Corallian sandstone deposition. Fault-controlled sedimentation of Corallian sediments in the Weald Basin was also proposed by de Wet (1998).

Fault activity led to localised water depth differences and, as a consequence, different styles of sedimentation between the Palmers Wood and Bletchingley (Fig.9 and 14). The common occurrence and lack of extended lateral correlation of both erosional and non-depositional discontinuities in all three wells suggests local changes in the creation of accommodation and sediment supply linked to local tectonic activity, rather than global sea level changes. Consequently, basinal facies associations south of the fault in BL5 emphasise the increasing water depth across the fault separating BL5 from PW3 and PW7 (Figs. 8 and 14).

The overall accumulation of facies in the three wells is typical of fault-controlled, marine sediment accumulation (Castro et al., 2019; de Wet, 1998). The irregular arrangement of coarsening and fining upward cycles (Figs. 5, 6 and 7), as well as the short-range vertical juxtaposition of facies associations (e.g., Sun (1992) in the top sand package S3 in BL5 (Fig.9), suggest transient changes in water depths as coarsening upward cycles indicate shoaling while fining upward cycles indicate flooding (Newell, 2000; Walker and Plint, 1992). The non-contiguous succession of facies associations in S3, as well as the absence of local correlation with other sand packages in the other wells required local variations in accommodation and sediment supply (de Wet, 1998), typical of aperiodic, allocyclic, tectonic controls (Cecil, 2013).

5.5 Climatic controls on sediment supply and deposition

The occurrence of coarse clastic Corallian deposits suggests a significant influence of hinterland weathering, run-off, and fluvial discharge into the marine environment (Leeder et al., 1998; Ruffell and Rawson, 1994) at the sites of Bletchingley and Palmers Wood. The distance of these fields from the London platform source area (Fig. 1), and the presence of products of hinterland weathering such as detrital kaolinite (Figs. 11 and 12), as well as mineralogical and textural maturity, are further indicators of continental weathering and fluvial transport.

Climatic conditions in the hinterland,-the London Platform,- that supplied the sediment are here inferred from mineralogical proxies which suggest warm, humid conditions with high rainfall. These mineralogical proxies include (i) kaolinite in detrital clay (Figs. 11B, 11D and 12B), (ii) presence of the iron-rich minerals, siderite and berthierine (Fig.11D), (iii) the absence of evaporite minerals or alkali-rich clays such as smectite (McKinley et al., 2003).

Kaolinite typically is produced in warm tropical to sub-tropical climates with high rainfall rates and vegetation (Burley and Worden, 2003). The decay of organic matter under humid conditions creates acidity which enhances chemical weathering of feldspar- and mica-bearing silicate rocks to produce kaolinite (Burley and Worden, 2003; Hallam, 1975).

The presence of siderite and berthierine in marine sediment indicates warm, humid, continental weathering because the formation of shallow marine iron-rich minerals requires intense weathering of continental rocks under humid conditions to form lateritic soils, which are then eroded and the iron transported to the marine environment (Hallam, 1984; Tucker, 1981). The presence of kaolinite (Worden and Burley, 2003) and the abundance of Fe-rich minerals (Worden et al., 2020), is here taken to show that advanced weathering in the hinterland occurred in organic-rich soils that resulted from lush vegetation.

The absence of evaporite minerals in these marine Corallian rocks precludes deposition on an arid shoreline, because evaporite minerals require subaerial concentration of dissolved salts, typical of arid conditions (Tucker, 1981). The absence of Ca^{2+} and Mg^{2+} clays, such as smectite, also seems to preclude arid conditions, as high rainfall typically causes intense leaching of alkaline and alkaline earth cations thereby reducing alkaline conditions and reducing the possibility of the creation and deposition Ca^{2+} and Mg^{2+} clay minerals (Burley and Worden, 2003; Sladen and Batten, 1984).

In summary, the climatic controls on sediment transport further provide an insight into the geology and weathering characteristics of the hinterland London Platform. As the Corallian sandstones are relatively shallow buried, we can infer their source-area characteristics as they have not had their depositional character overprinted by burial (meso) diagenesis (Sladen and Batten, 1984). We can therefore infer that the Upper Jurassic London platform created mature sediments which resulted from advanced weathering in a warm humid environment. The material deposited as the Corallian sandstones was transported from a warm vegetated hinterland, with substantial rainfall , capable of causing fluvial transport of sediments which were deposited in a shallow marine environment.

5.6 Controls on reservoir quality

From a sedimentological perspective, all three wells have well-defined sand packages (Figs. 5, 6, 7, 8 and 9). From core examination, the elevated degree of hydrocarbon staining in the less cemented sandstone zones (Figs. 3A and B) indicates that calcite cementation is a significant control on reservoir quality. Calcite cement is present in variable amounts throughout the cores and seems to display no distinct relationship with sedimentary structures, lithology or bioturbation (Figs. 5, 6 and 7). Analysis of log-derived porosity for each well, subdivided by facies association, shows that there is apparently no simple relationship between porosity and depositional facies association (Fig. 13A). This is because the trend of high and low porosity is not consistent with facies associations, as seen in Figure 13. For instance, the upper shoreface facies association has porosity above the mean value in BL5, below the mean value in PW3 and slightly above the mean value in PW7 (Fig. 13A).

Comparison of sedimentary logs to log-derived porosity and oil saturation, for all three wells (Figs. 5 to 7), confirms that there is no simple relationship between grain size and porosity. For example, the elevated porosity in PW3 at 1090.9m is associated with finer-grained sandstones than the lower porosity-bed immediately below (Fig. 6). In all wells, the fluctuations in porosity in the sandstones above and below the intra-Corallian mudstone are not linked to variations in the proportion of clay minerals, as revealed by the interpreted shale volumes in Figures 5 to 7. The 10 to20 % variations in Corallian sandstone porosity must be due to another process. The core-derived estimation of intensity of cementation (weakly, moderately or highly calcite cemented) links well with the wireline-log-derived estimation of porosity with the highest porosity values tied to weakly or moderately cemented sandstones. The low porosity beds in the Corallian sandstones are all highly calcite cemented.

The anomalous extra sandstone interval (S3) at the top of the Corallian in BL5 is unusual in that it has uniformly poor reservoir quality; the high porosity values typical of the sandstones either side of the intra-Corallian are absent (Fig. 7). There are two possible explanations for the poor reservoir quality. First is that the shale proportion in S3 never gets lower than 10 % and is more typically 20 %. Second is that core description showed that the whole of the anomalous top sandstone layer in BL5 is highly calcite cemented.

The intra-Corallian, defined by the high shale proportion, also tends to be highly calcite cemented (Figs. 5 - 7) suggesting that this correlatable unit will act as a baffle or a barrier to fluid movement due to the abundance of both clay minerals and carbonate cement.

Petrographic analysis confirms the combined interpretation of core and wireline logs, as it revealed that calcite cement is the dominant pore-filling mineral (Fig. 10) with the most porous samples having the least quantities of calcite cement (Fig. 11A). SEM-EDS analysis revealed that median calcite volumes are relatively high (9% to 39%), but the interquartile ranges are large confirming that calcite cement is heterogeneously distributed (Fig. 13B). The Corallian sandstones do not display signs of advanced compaction, with an absence of long grain contacts and occurrence of a floating-grain texture (Fig. 10B and11A) suggesting that mechanical compaction did not play a major role in porosity-loss and proving the role of cementation in reservoir quality evolution. Petrographic examination revealed that clay minerals occupy pore space as matrix, especially in the finer grained samples (Fig. 12) showing that the presence of clay minerals has also caused reduction in reservoir quality. SEM-EDS analysis confirmed that median clay mineral volumes are relatively low (1 % to 2 %) but high upper quartile ranges shows that it is locally present at high concentrations (Fig. 13C).

5.7 Influence of depositional controls on reservoir quality

Depositional controls have two effects on reservoir quality and reservoir architecture: (1) stratigraphic controls caused by sea level rise as seen in the intra-Corallian: this caused compartmentalisation of the reservoirs into upper and lower units, (2) regional lateral controls caused by tectonism, as seen in the additional (anomalous) uppermost sand package (S3) in BL5 as well as the elevated clay content in BL5 (Figs. 8, 13 and14)

Syn-depositional tectonism in the Weald Basin, with predominantly downthrown faults to the south is interpreted to have caused an increase in water depth south of the fault, as indicated by the greater prevalence of lower energy, deeper water, facies associations in BL5 compared to PW3 and PW7 (Fig. 9). The increase in water depth is interpreted to have had three effects: (1) potential recycling of sediments from the upthrown side (PW3 and PW7) to the downthrown side (BL5) (Fig. 14), (2) increase in accommodation space leading to the deposition of a thicker Corallian section in BL5 (Figs. 8 and 14) and (3) reduction in energy leading to the deposition of finer-grained, lower energy facies associations (Fig.9) as well as fewer bioclasts (Fig. 13D). From a reservoir quality perspective, porosity decreases across the fault from an average 12% in PW7 and 13% in PW3 to 8% in BL5 (Fig. 13A). However, BL5 has the lowest quantity of calcite of the three wells (Fig. 13B) with a mean of only 9.3 % as against PW3's 38.9 % and PW7's 22.3 %. The difference in calcite quantity is interpreted to be a consequence of the reduction in energy in the depositional environment across the fault, hence a reduction in capacity to transport bioclasts that then neomorphosed to calcite cement (Adams, 1998; Scotchman et al., 1989; Worden et al., 2019).

6. Conclusion

1. In the Palmers Wood and Bletchingley area of the Weald Basin, the majority of the Corallian sandstones were deposited as two distinct sand bodies separated by a flooding surface, represented by an intra-Corallian mud- and silt-stone section. Both upper and lower sand bodies have numerous coarsening upward cycles, characteristic of highstand conditions, where sediment supply outpaced base-level rise during normal regression conditions. The absence of paleosols, rhizocretions or terrestrial ichnofossils suggests emergence did not happen and support and interpretation of deposition under highstand conditions with sediment supply transiently outpacing eustatic sea level rise. The major evidence for a eustatic influence on deposition is the intra-Corallian fine-grained section and flooding surface which suggests a major allostratigraphic event caused by base level rise outpacing sediment supply.

2. Evidence of a tectonic influence on the Corallian sandstones include non-correlation of erosional and hiatal surfaces across a major E-W fault, non-contiguous facies associations and thickening of the Corallian sandstone across the fault.

3. Climatic conditions during weathering and transport of the Corallian sediments, from the hinterland inthe north are here interpreted to have been warm and humid with abundant vegetation. These conditions were responsible for the accumulation of iron-rich, sand-dominated sediment that may have been nutrient-rich, thus encouraging the intense bioturbation typical of the Corallian clastic sediments.

4. There is not a strong relationship between facies association and reservoir quality. Depositional controls, however, influenced reservoir quality distribution and reservoir architecture. The sandstone reservoir units are compartmentalised into an upper and lower unit by eustatic controls. Tectonism caused the increase in net thickness of the sandstone units in BL5. Tectonism also caused the horizontal separation of the sandstone unit S3 from the other reservoir sections and the reservoir quality is somewhat poorer across the fault in BL5 which has a slightly higher clay content than the Palmers Wood wells, caused by tectonism.

5. Reservoir quality variations, in these shallow buried sandstones, are largely controlled by the variable abundance of calcite cement. The best reservoir quality is associated with the lowest amounts of calcite cement. Calcite cement abundance is directly linked to the proportion of primary calcareous bioclasts revealing that autogenic controls dominate reservoir quality.

Acknowledgements

We wish to thank the British Geological Survey at Keyworth, Nottinghamshire, for access to the Palmers Wood and Bletchingley cores. We thank staff from IGas for providing log and core data. We are also grateful to the Petroleum Technology Development Fund (PTDF) for funding this research. Petrographic analysis was carried out at the Diagenesis Research Group at the University of Liverpool and portable X-ray fluorescence spectrometry was also provided by the Central Teaching Labs (CTL) of the University of Liverpool. Thanks to James Utley of the Diagenesis Research Group for his help with petrographic analyses and finally to Robert Duller of the Department of Earth Ocean and Ecological Sciences University of Liverpool for his thoughtful ideas during the course of this study.

References

Adams, A., 1998. Carbonate sediments and rocks under the microscope: a colour atlas. Manson Publishing Ltd., London.

Allen, P.A., Underhill, J.R., 1989. Swaley cross-stratification produced by unidirectional flows, Bencliff Grit (Upper Jurassic), Dorset, UK. Journal of the Geological Society 146, 241-252.

Andrews, I., 2014. The Jurassic shales of the Weald Basin: geology and shale oil and shale gas resource estimation, in: DECC (Ed.). British Geological Survey, London UK, pp. 1-79.

Andrieu, S., Brigaud, B., Barbarand, J., Lasseur, E., Saucède, T., 2016. Disentangling the control of tectonics, eustasy, trophic conditions and climate on shallow-marine carbonate production during the Aalenian–Oxfordian interval: From the western France platform to the western Tethyan domain. Sedimentary Geology 345.

Arkell, W.J., 1933. The Jurassic System in Great Britain. Clarendon Press, Oxford.

Armitage, P.J., Worden, R.H., Faulkner, D.R., Aplin, A.C., Butcher, A.R., Iliffe, J., 2010. Diagenetic and sedimentary controls on porosity in Lower Carboniferous fine-grained lithologies, Krechba field, Algeria: A petrological study of a caprock to a carbon capture site. Marine and Petroleum Geology 27, 1395-1410.

Burley, S.D., Worden, R.H., 2003. Sandstone diagenesis. [electronic book] : recent and ancient. Malden, MA ; Blackwell Publishing, 2003.

Burton, R., Kendall, C.G.S.C., Lerche, I., 1987. Out of our depth: on the impossibility of fathoming eustasy from the stratigraphic record. Earth-Science Reviews 24, 237-277.

Butler, M., Pullan, C.P., 1990. Tertiary structures and hydrocarbon entrapment in the Weald Basin of southern England. Geological Society, London, Special Publications 55, 371-391.

Castro, H.R., Figueiredo, F.T., Franco, L.S., Gomes, P.V., Soares, I.R., Andrade, L.L., Ramos, M.A., Moraes, J.D., 2019. Facies distribution as a response to early rift tectonic activity in the Sergipe-Alagoas Basin, northeastern Brazil. Sedimentary geology 383, 216-237.

Cecil, C.B., 2013. An overview and interpretation of autocyclic and allocyclic processes and the accumulation of strata during the Pennsylvanian–Permian transition in the central Appalachian Basin, USA. International Journal of Coal Geology 119, 21-31.

Chadwick, R., 1985a. Cenozoic sedimentation, subsidence and tectonic inversion, in: Whittaker, A. (Ed.), Atlas of Onshore Sedimentary Basins in England and Wales. Blackie, Glasgow, pp. 61-63.

Chadwick, R., 1985b. Permian, Mesozoic and Cenozoic structural evolution of England and Wales in relation to the principles of extension and inversion tectonics, in: Whittaker, A. (Ed.), Atlas of onshore sedimentary basins in England and Wales: Post-Carboniferous tectonics and stratigraphy. Blackie, Glasgow, pp. 9-25.

Chadwick, R., 1993. Aspects of basin inversion in southern Britain. Journal of the Geological Society 150, 311-322.

Childs, C., Nicol, A., Walsh, J.J., Watterson, J., 2003. The growth and propagation of synsedimentary faults. Journal of Structural Geology 25, 633-648.

Conybeare, C.E.B., 2013. Lithostratigraphic analysis of sedimentary basins. Academic Press, New York.

Dailly, G., 1975. Some remarks on regression and transgression in deltaic sediments, in: Yorath, C.J., Parker, E.R., Glass, D.J. (Eds.), Canada's Continental Margins and Offshore Petroleum Exploration. Canadian Society of Petroleum Geologists, Calgary, Alberta, Canada, pp. 791-820.

de Wet, C.B., 1987. Deposition and diagenesis in an extensional basin: the Corallian Formation (Jurassic) near Oxford, England. Geological Society, London, Special Publications 36, 339-353.

de Wet, C.B., 1998. Deciphering the sedimentological expression of tectonics, eustasy, and climate: a basinwide study of the Corallian Formation, southern England. Journal of Sedimentary Research 68, 653-667.

Downing, R.A., Allen, D.J., Barker, J.A., Burgess, W.G., Gray, D.A., Price, M., Smith, I.F., 1983. Geothermal Exploration at Southampton in the UK: A Case Study of a Low Enthalpy Resource. Energy Explor. Exploit. 2, 327-342.

Ebukanson, E.J., 1984. An investigation of some potential Jurassic hydrocarbon source rocks of Southern England. University of London.

Farrell, K.M., Harris, W.B., Mallinson, D.J., Culver, S.J., Riggs, S.R., Pierson, J., Self-Trail, J.M., Lautier, J.C., 2012. Standardizing texture and facies codes for a process-based classification of clastic sediment and rock. Journal of Sedimentary Research 82, 364-378.

Goldring, R., Astin, T.R., Marshall, J.E.A., Gabbott, S., Jenkins, C.D., 1998. Towards an integrated study of the depositional environment of the Bencliff Grit (Upper Jurassic) of Dorset, in: Underhill, J.R. (Ed.), Development, Evolution and Petroleum Geology of the Wessex Basin, pp. 355-372.

Gowland, S., 1996. Facies characteristics and depositional models of highly bioturbated shallow marine siliciclastic strata: An example from the Fulmar Formation (Late Jurassic), UK Central Graben. Geological Society, London, Special Publications 114, 185-214.

Griffiths, J., Worden, R.H., Wooldridge, L.J., Utley, J.E.P., Duller, R.A., 2019. Compositional variation in modern estuarine sands: Predicting major controls on sandstone reservoir quality. American Association of Petroleum Geologists Bulletin 103, 797-833.

Hallam, A., 1975. Jurassic environments. Cambridge University Press, Cambridge.

Hallam, A., 1977. Jurassic bivalve biogeography. Paleobiology 3, 58-73.

Hallam, A., 1978. Eustatic cycles in the Jurassic. Palaeogeography, Palaeoclimatology, Palaeoecology 23, 1-32.

Hallam, A., 1981. A revised sea-level curve for the early Jurassic. Journal of the Geological Society 138, 735-743.

Hallam, A., 1984. Continental humid and arid zones during the jurassic and cretaceous. Palaeogeography, Palaeoclimatology, Palaeoecology 47, 195-223.

Hampson, G.J., Storms, J.E., 2003. Geomorphological and sequence stratigraphic variability in wave-dominated, shoreface-shelf parasequences. Sedimentology 50, 667-701.

Hansen, D.L., Blundell, D.J., Nielsen, S.B., 2002. A model for the evolution of the Weald Basin. Bulletin of the Geological Society of Denmark 49, Part 2, 109-118.

Haq, B.U., 2017. Jurassic sea-level variations: a reappraisal. GSA Today 28, 4-10.

Hardenbol, J., Thierry, J., Farley, M.B., Jacquin, T., De Graciansky, P.-C., Vail, P.R., 1998. Mesozoic and Cenozoic sequence chronostratigraphic framework of European basins. Society of Economic Paleontologists and Mineralogists Special Publication 60, 3-13.

Hawkes, P.W., Fraser, A.J., Einchcomb, C.C.G., 1998. The tectono-stratigraphic development and exploration history of the Weald and Wessex basins, Southern England, UK. Geological Society, London, Special Publications 133, 39-65.

Heasley, E.C., Worden, R.H., Hendry, J.P., 2000. Cement distribution in a carbonate reservoir: recognition of a palaeo oil-water contact and its relationship to reservoir quality in the Humbly Grove field, onshore, UK. Marine and Petroleum Geology 17, 639-654.

Hillis, R., Holford, S., Green, P., Dore, A., Gatliff, R., Stoker, M., Thomson, K., Turner, J., Underhill, J., Williams, G., 2008. Cenozoic exhumation of the southern British Isles. Geology 36.

Hogg, A.J.C., Mitchell, A.W., Young, S., 1996. Predicting well productivity from grain size analysis and logging while drilling. Petroleum Geoscience 2, 1-15.

Jones, D.K., 1999. On the uplift and denudation of the Weald, in: Hartey, A.J., Holdsworth, R.E., Morton, A.C., Stoker, M.S. (Eds.), Uplift, Erosion and Stability: Perspectives on Long-term Landscape Development Geological Society, London, Special Publications, London, pp. 25-43.

Kamola, D.L., Van Wagoner, J.C., 1995. Stratigraphy and facies architecture of parasequences with examples from the Spring Canyon Member, Blackhawk Formation, Utah, in: Wagoner, J.C., Bertram, G.T. (Eds.), Sequence Stratigraphy of Foreland Basin Deposits: Outcrop and Subsurface Examples from the Cretaceous of North America. American Association of Petroleum Geologists memoir 64, Tulsa, Oklahoma, pp. 27-54.

Kupecz, J.A., Gluyas, J.G., Bloch, S., Geologists, A.A.o.P., 1997. Reservoir Quality Prediction in Sandstones and Carbonates. American Association of Petroleum Geologists.

Lake, S.D., Karner, G.D., 1987. The structure and evolution of the Wessex Basin, southern England: an example of inversion tectonics. Tectonophysics 137, 347-378.

Law, A., 1998. Regional uplift in the English Channel: quantification using sonic velocity, in: Underhill, J.R. (Ed.), Development, Evolution and Petroleum Geology of the Wessex Basin. Geological Society, London, Special Publications, pp. 187-197.

Lawrence, D.T., 1993. Evaluation of Eustasy, Subsidence, and Sediment Input as Controls on Depositional Sequence Geometries and the Synchroneity of Sequence Boundaries, in: Weimer, P., Posamentier, H.W. (Eds.), Siliciclastic Sequence Stratigraphy: Recent Developments and Applications. American Association of Petroleum Geologists memoir 58, Tulsa, Oklahoma, pp. 337-368.

Leeder, M.R., Harris, T., Kirkby, M.J., 1998. Sediment supply and climate change: implications for basin stratigraphy. Basin research 10, 7-18.

McBride, E., 1963. A Classification of Common Sandstones. Journal of Sedimentary Research 33, 664-669.

McKinley, J., Worden, R. H, Ruffell, A., 2003. Smectite in sandstones: a review of the controls on occurrence and behaviour during diagenesis, in: Worden, R.H., Morad, S. (Eds.), Clay mineral cements in sandstones. International Association of Sedimentologists, Special Publications 34, pp. 109-128.

Newell, A.J., 2000. Fault activity and sedimentation in a marine rift basin (Upper Jurassic, Wessex Basin, UK). Journal of the Geological Society 157, 83-92.

Palci, F., Fraser, A., Carles, M., Neumaier, M., Sanderson, S., Wallace, R., 2018. Unconventional Hydrocarbon Potential of the Weald Basin, Southern England, United Kingdom, AAPG ACE 2018. American Association of Petroleum Geologists, Salt Lake City, Utah.

Parrish, R., Parrish, C., Lasalle, S., 2018. Vein calcite dating reveals Pyrenean orogen as cause of Paleogene deformation in southern England. Journal of the Geological Society 175, jgs2017-2107.

Pemberton, G., Maceachern, J., Dashtgard, S., Bann, K., Gingras, M., Zonneveld, J.-P., 2012. Shorefaces, in: Knaust, D., Bromley, R.G. (Eds.), Trace Fossils as Indicators of Sedimentary Environments. Developments in Sedimentology, pp. 563-603.

Pirrie, D., Butcher, A.R., Power, M.R., Gottlieb, P., Miller, G.L., 2004. Rapid quantitative mineral and phase analysis using automated scanning electron microscopy (QemSCAN): Potential applications in forensic geoscience, in: Pye, K., Croft, D.J. (Eds.), Forensic Geoscience: Principles, Techniques and Applications. Geological Society, Bath, pp. 123-136.

Posamentier, H.W., Vail, P.R., 1988. Eustatic Controls on Clastic Deposition II—Sequence and Systems Tract Models, in: Wilgus, C.K., Hastings, B.S., Ross, C.A., Posamentier, H.W., Van Wagoner, J., Kendall, C.G.S.C. (Eds.), Sea-Level Changes: An Integrated Approach. Society for Sedimentary Geology, pp. 125-154.

Rahman, M.J.J., Worden, R.H., 2016. Diagenesis and its impact on the reservoir quality of Miocene sandstones (Surma Group) from the Bengal Basin, Bangladesh. Marine and Petroleum Geology 77, 898-915.

Ruffell, A.H., Rawson, P.F., 1994. Palaeoclimate control on sequence stratigraphic patterns in the late Jurassic to mid-Cretaceous, with a case study from Eastern England. Palaeogeography, Palaeoclimatology, Palaeoecology 110, 43-54.

Salah, M.K., El Ghandour, M.M., Abdel-Hameed, A.M.T., 2016. Effect of diagenesis on the petrophysical properties of the Miocene rocks at the Qattara Depression, north Western Desert, Egypt. Arab. J. Geosci. 9.

Schmid, S., Worden, R.H., Fisher, Q.J., 2004. Diagenesis and reservoir quality of the Sherwood Sandstone (Triassic), Corrib Field, Slyne Basin, west of Ireland. Marine and Petroleum Geology 21, 299-315.

Scholle, P.A., Ulmer-Scholle, D.S., 2003. A Color Guide to the Petrography of Carbonate Rocks: Grains, Textures, Porosity,Diagenesis. American Association of Petroleum Geologists memoir, Tulsa, Oklahoma.

Scotchman, I., Johnes, L., Miller, R., 1989. Clay diagenesis and oil migration in Brent Group sandstones of NW Hutton Field, UK North Sea. Clay Minerals 24, 339-374.

Scotese, C.R., 2001. Atlas of earth history. PALEOMAP project.

Seilacher, A., 1967. Bathymetry of trace fossils. Marine geology 5, 413-428.

Sellwood, B.W., Scott, J., Lunn, G., 1986. Mesozoic basin evolution in Southern England. Proceedings of the Geologists' Association 97, 259-289.

Sladen, C., Batten, D., 1984. Source-area environments of Late Jurassic and Early Cretaceous sediments in southeast England. Proceedings of the Geologists' Association 95, 149-163.

Sun, S.Q., 1989. A new interpretation of the Corallian (Upper Jurassic) cycles of the Dorset coast, southern England. Geological Journal 24, 139-158.

Sun, S.Q., 1992. A storm-dominated offshore sandstone interval from the Corallian Group (Upper Jurassic), Weald Basin, southern England. Marine and Petroleum geology 9, 274-286.

Talbot, M.R., 1973. Major sedimentary cycles in the corallian beds (Oxfordian) of Southern England. Palaeogeography, Palaeoclimatology, Palaeoecology 14, 293-317.

Taylor, A., Goldring, R., 1993. Description and analysis of bioturbation and ichnofabric. Journal of the Geological Society 150, 141-148.

Taylor, S.P., Sellwood, B.W., Gallois, R.W., Chambers, M.H., 2001. A sequence stratigraphy of the Kimmeridgian and Bolonian stages (late Jurassic): Wessex–Weald Basin, southern England. Journal of the Geological Society 158, 179-192.

Trueman, S., 2003. The Humbly Grove, Herriard, Storrington, Singleton, Stockbridge, Goodworth, Horndean, Palmers Wood, Bletchingley and Albury Fields, Hampshire, Surrey and Sussex, UK Onshore, in: Gluyas, J.G., Hichens, H.M. (Eds.), United Kingdom Oil and Gas Fields Commemorative Millennium Volume. Geological Society, Memoirs, London, pp. 929-941.

Tucker, M., 1981. Sedimentary petrology: an introduction. Blackwell Scientific Publications, Oxford.

Vakarelov, B.K., Ainsworth, R.B., MacEachern, J.A., 2012. Recognition of wave-dominated, tide-influenced shoreline systems in the rock record: Variations from a microtidal shoreline model. Sedimentary Geology 279, 23-41.

Wagoner, J.C., Mitchum, R.M., Campion, K., Rahmanian, V.D., 1990. Siliciclastic sequences in well logs, cores and outcrops: Concepts for High-Resolution Correlation of Time and Facies, in: Wagoner, J.C. (Ed.), Methods In Exploration Series. American Association of Petroleum Geologists, Tulsa, Oklahoma.

Walker, R.G., James, N.P., 1992. Facies models: Response to sea-level change: Geological Association of Canada. Geotext 1, 409.

Walker, R.G., Plint, G., 1992. Wave-and Storm-Dominated Shallow Marine Systems., in: Walker, R.G., James, N.P. (Eds.), Facies Models: A response to Sea Level Change. Geological Association of Canada, Newfoundland, pp. 219-238.

Wooldridge, L.J., Worden, R.H., Griffiths, J., Utley, J.E.P., 2018. The origin of clay-coated sand grains and sediment heterogeneity in tidal flats. Sedimentary Geology 373, 191-209.

Worden, R.H., Armitage, P.J., Butcher, A., Churchill, J., Csoma, A., Hollis, C., Lander, R.H., Omma, J., 2018. Petroleum reservoir quality prediction: overview and contrasting approaches from sandstone and carbonate communities, in: Armitage, P.J., Butcher, A., Churchill, J., Csoma, A., Hollis, C., Lander, R.H., Omma, J., Worden, R.H. (Eds.), Reservoir Quality of Clastic and Carbonate Rocks: Analysis, Modelling and Prediction. Special Publication. Geological Society, London, pp. 1-31.

Worden, R.H., Burley, S.D., 2003. Sandstone diagenesis: the evolution from sand to stone, in: Burley, S.D., Worden, R.H. (Eds.), Sandstone diagenesis, recent and ancient. International Association of Sedimentologists Reprint Series, pp. 3-44.

Worden, R.H., Griffiths, J., Wooldridge, L.J., Utley, J.E.P., Lawan, A.Y., Muhammed, D.D., Simon, N., Armitage, P.J., 2020. Chlorite in sandstones. Earth Science-Reviews 204, 103105.

Worden, R.H., Morrall, G.T., Kelly, S., Mc Ardle, P., Barshep, D.V., 2019. A renewed look at calcite cement in marine-deltaic sandstones: the Brent Reservoir, Heather Field, northern North Sea, UK. Geological Society, London, Special Publications 484, SP484-2018-2043.

Wright, J.K., 1981. The Corallian rocks of north Dorset. Proceedings of the Geologists' Association 92, 17-32.

Figure captions

Fig. 1: Location map of the study area giving the surface geology with inset at the top-left showing the map of England and the case study location (1A). The top –right area shows the an enlargement of the study location highlighting faults separating the Palmers Wood and Bletchingley Fields. (1B)Schematic subsurface section and major structural trends as adapted from Andrews (2014); Butler and Pullan (1990); Trueman (2003). Structures in the Weald Basin show a general east-west trend, one of these (marked in the rectangle to the north) is the east-west fault separating Palmers Wood and Bletchingley fields (1A).

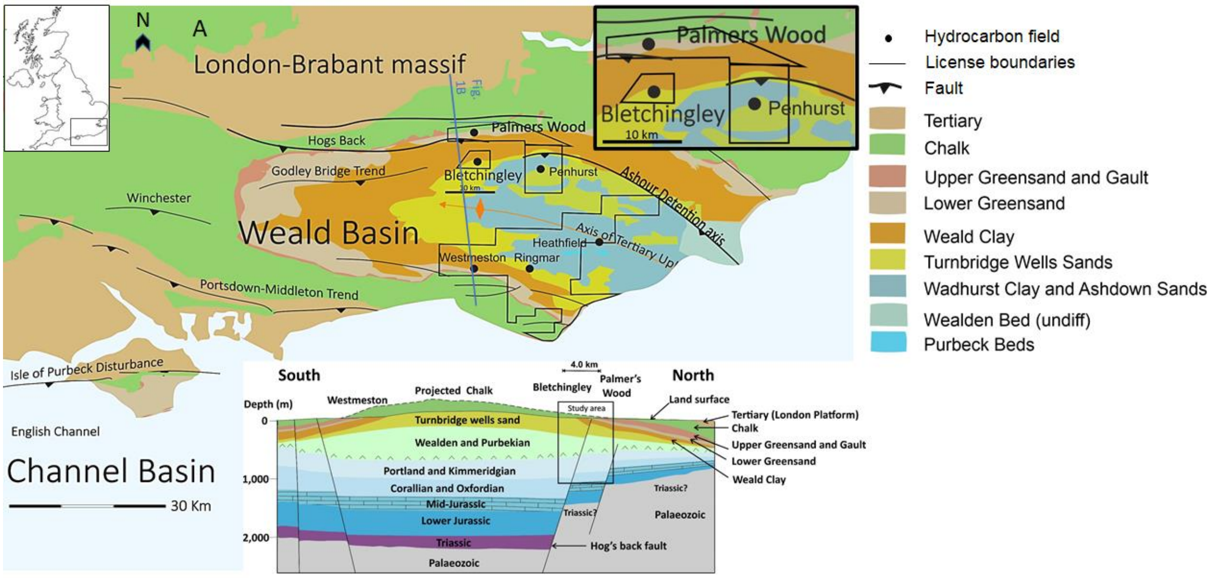

Fig.1

Fig. 2: (A) Stratigraphy of the Weald Basin, modified from Butler and Pullan (1990),showing major tectonic episodes and lithologic units with the Corallian section highlighted by the rectangle in the Upper Jurassic. The section show the Corallian sandstones deposited during a period of tectonic activity accompanied by graben development and regional subsidence. The Corallian has been described as both a group (Wright, 1981) and a formation (de Wet, 1998). Here we have adopted the term Corallian Formation to match the naming of the under- and overlying Oxford Clay and Kimmeridge Clay Formations. (B) Jurassic sea level curves, modified from Haq (2017), show dominant sea level rise through the late Jurassic with the dotted rectangle showing the time that the Corallian sandstone was deposited. Sequence boundaries define rapid seaward shoreline movements corresponding to minor sea level falls punctuating an overall landward shoreline movement. (C) This is a stratigraphic section summarising the Corallian Group as modified from Sun (1992). The Corallian sandstone Formation is highlighted at the top of the Corallian Group.

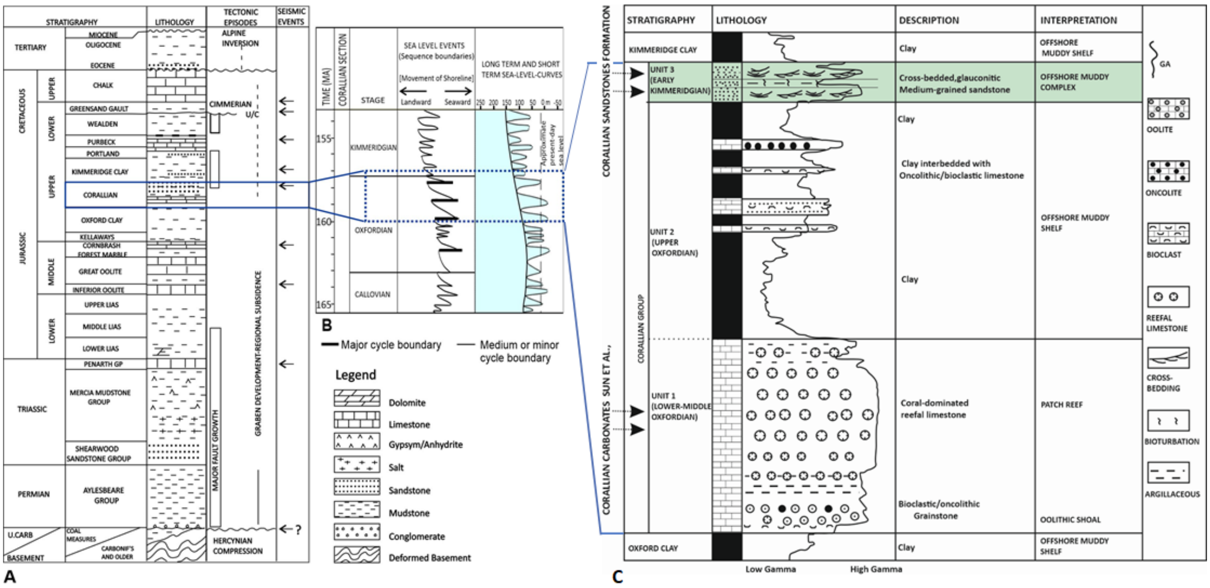

Fig. 3: (A) PW3 (1090.6-1090.9) highly cemented foreshore sandstone with no visible bioturbation (B) PW7 (1131.6) loosely cemented medium-grained, massive bedded upper shoreface sandstone with no visible bioturbation. The brown colour is from intense hydrocarbon staining. (C) BL5 (2207.5 m to 2207.9 m) proximal lower shoreface sandstones has been intensely bioturbated obscuring original fabric (BL5 is deviated at an angle of about 50°, explaining the great difference in measured depths). (D) PW3 (1087.9 m) distal lower shoreface sandstones, beds show rapid colonisation after a storm event. The broken line shows an erosional surface at the top of the storm bed. The non-amalgamated coarse-grained bed at the middle is succeeded by an argillaceous low energy section with parallel lamination (S pl) and increase in bioturbation. (E) PW3 (1098.5 m) offshore muds with laminated silty lenses. Lenses have parallel lamination (S pl) and wave ripple lamination (S r-lam). *Anconichnus (An), Asterosoma (As),*bivalve (bi) shells, *Chondrites (Ch), Ophiomorpha (O), Paleophycus (Pa), Planolites*(P),*Diplocraterion habichi(Dh), Skolithos (S), Teichichnus (T), Terebellina (Te)* and *Thalasinoides (Th).*

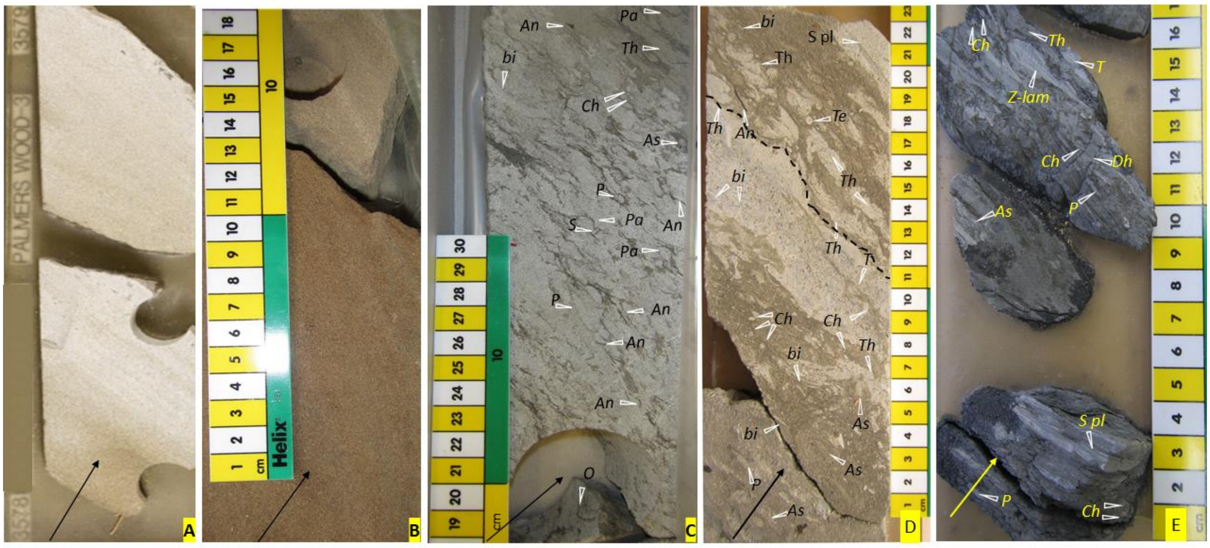

Fig. 4: The key for the sedimentary logs in figures 5, 6 and 7.

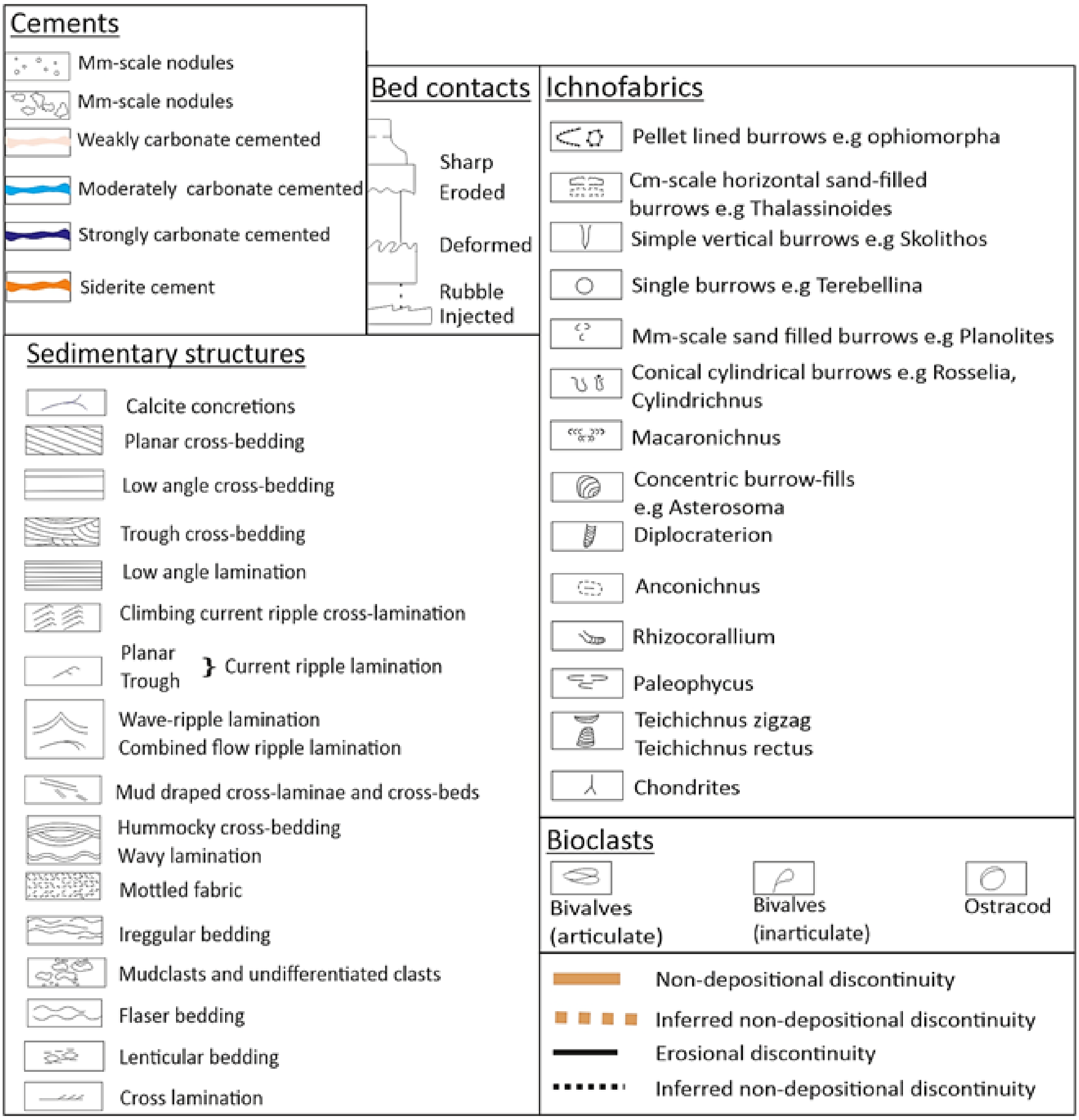

Fig. 5: Detailed sedimentary log, wireline lithology log, and neutron-density cross-over plots for PW7: (A) sedimentary structures, extent of cementation, facies associations, bioturbation and discontinuities. (B) the lithology interpretation from wireline logs with relative proportions of oil saturation, sandstone, shale and water. (C) a neutron-density cross-over plot with non-pay zones coloured brown and pay zones coloured yellow. The sedimentary log shows the Corallian sandstones separated by a local argillaceous section. The sedimentary logs also show coarsening upward cycles interrupted by a fining upward cycle (top of B and lower part of A). Common discontinuities point to a varied interplay of energy levels and/or sediment source. The lithology log shows good sand/shale correlation with grain size variation and bioturbation (when grain size does not change). Also note the increase in porosity in the top and bottom argillaceous sections. Wireline depths have been shifted to match core.

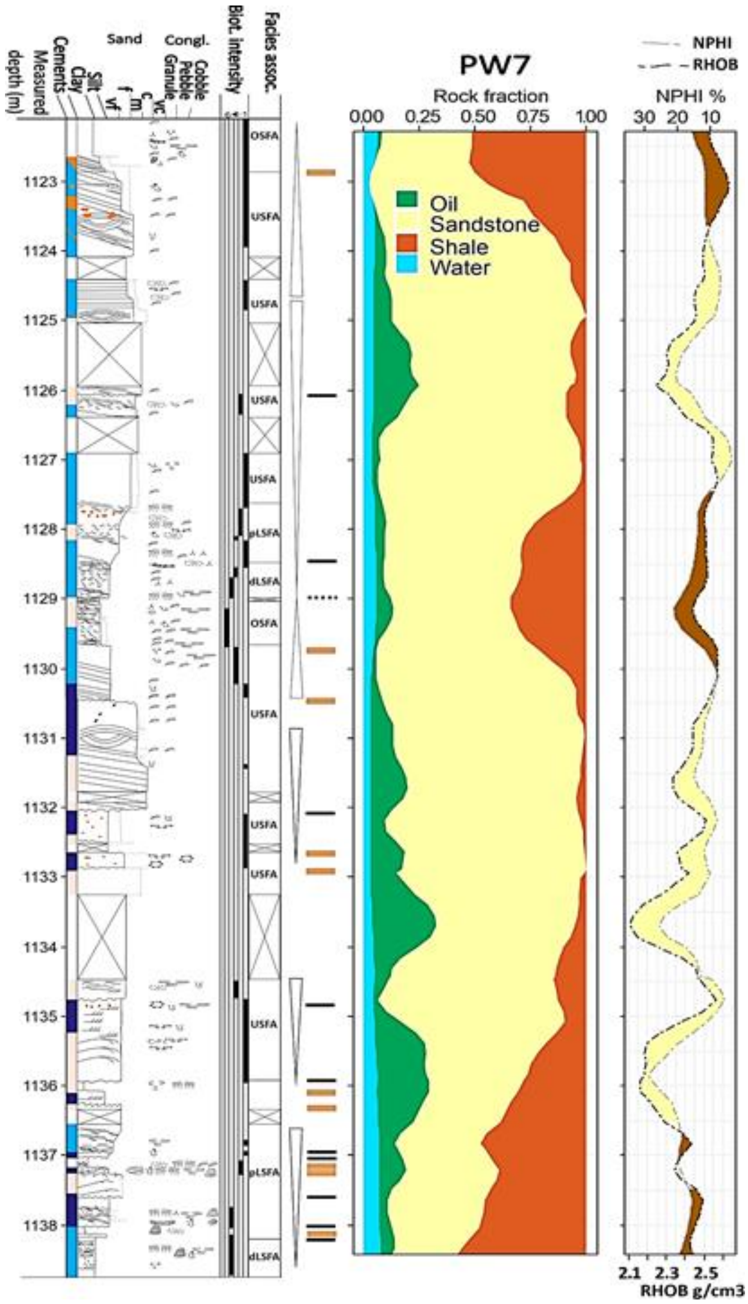

Fig. 6: Detailed sedimentary log, wireline lithology log, and neutron-density cross-over plots for PW3: (A) sedimentary structures, extent of cementation, facies associations, bioturbation and discontinuities. (B) the lithology interpretation from wireline logs with relative proportions of oil saturation, sandstone, shale and water. (C) a neutron-density cross-over plot with non-pay zones coloured brown and pay zones coloured yellow. In the sedimentary log beds show frequent short-range facies shifts with mostly upper shoreface facies association truncated by lower energy facies associations. The middle argillaceous section does not show change in grain size but has been highly bioturbated. Wireline depths have been shifted to match core depths.

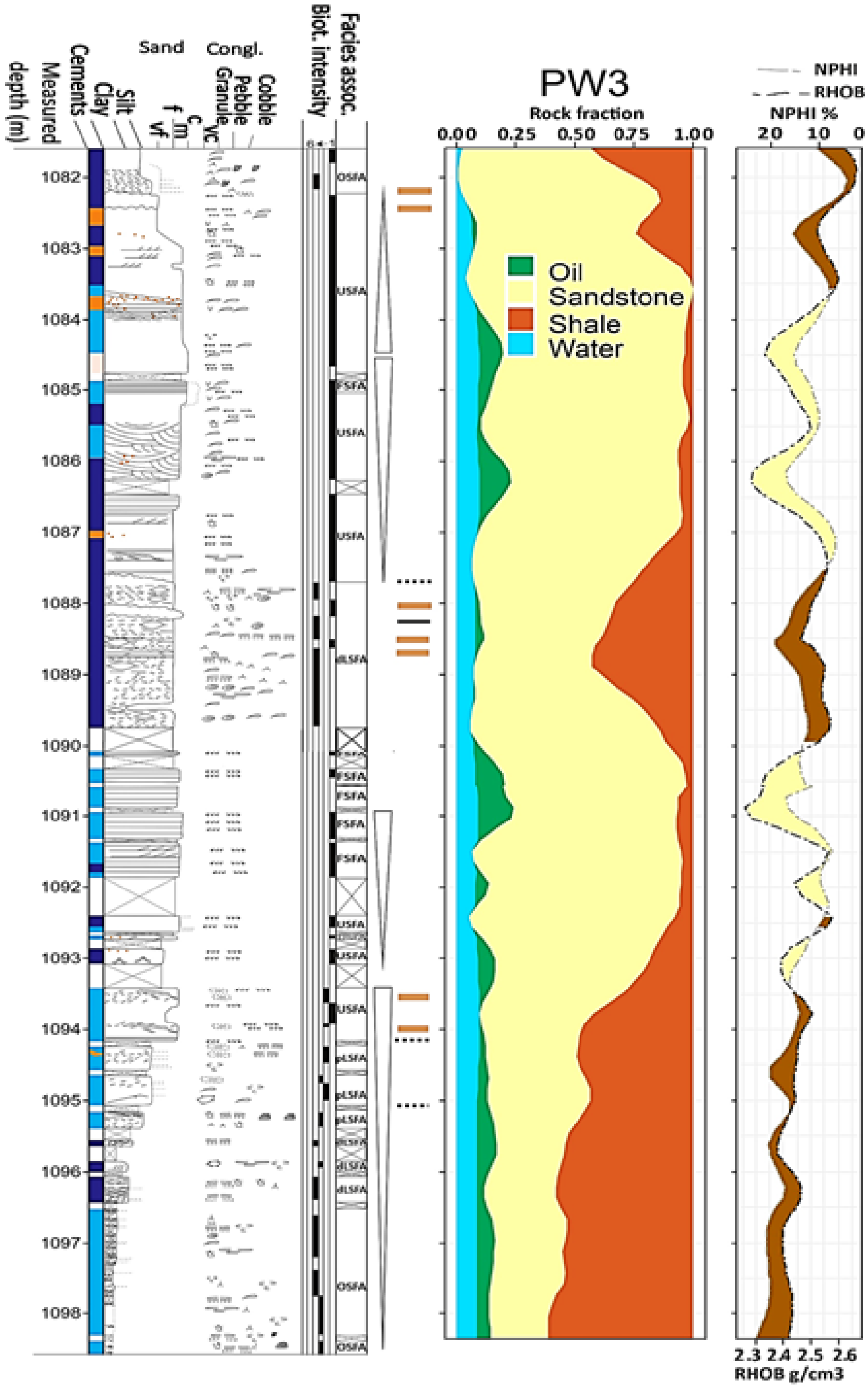

Fig. 7: Detailed sedimentary log, wireline lithology log, and neutron-density cross-over plots for BL5: (A) sedimentary structures, extent of cementation, facies associations, bioturbation and discontinuities. (B) the lithology interpretation from wireline logs showing relative proportions of oil saturation, sandstone, shale and water. (C) a neutron-density cross-over plot with Non-pay zones coloured brown and pay zones coloured yellow. Note that BL5 has another argillaceous section from 2201.9 m to 2199.4 m. Several coarsening and fining upwards cycles are observed and argillaceous sections are more common in this well compared to the Palmers Wood wells. The log also shows common erosional and non-depositional discontinuities, and short-range vertical heterogeneity in cementation and sedimentary structures. Wireline depths have been shifted to match core depths.

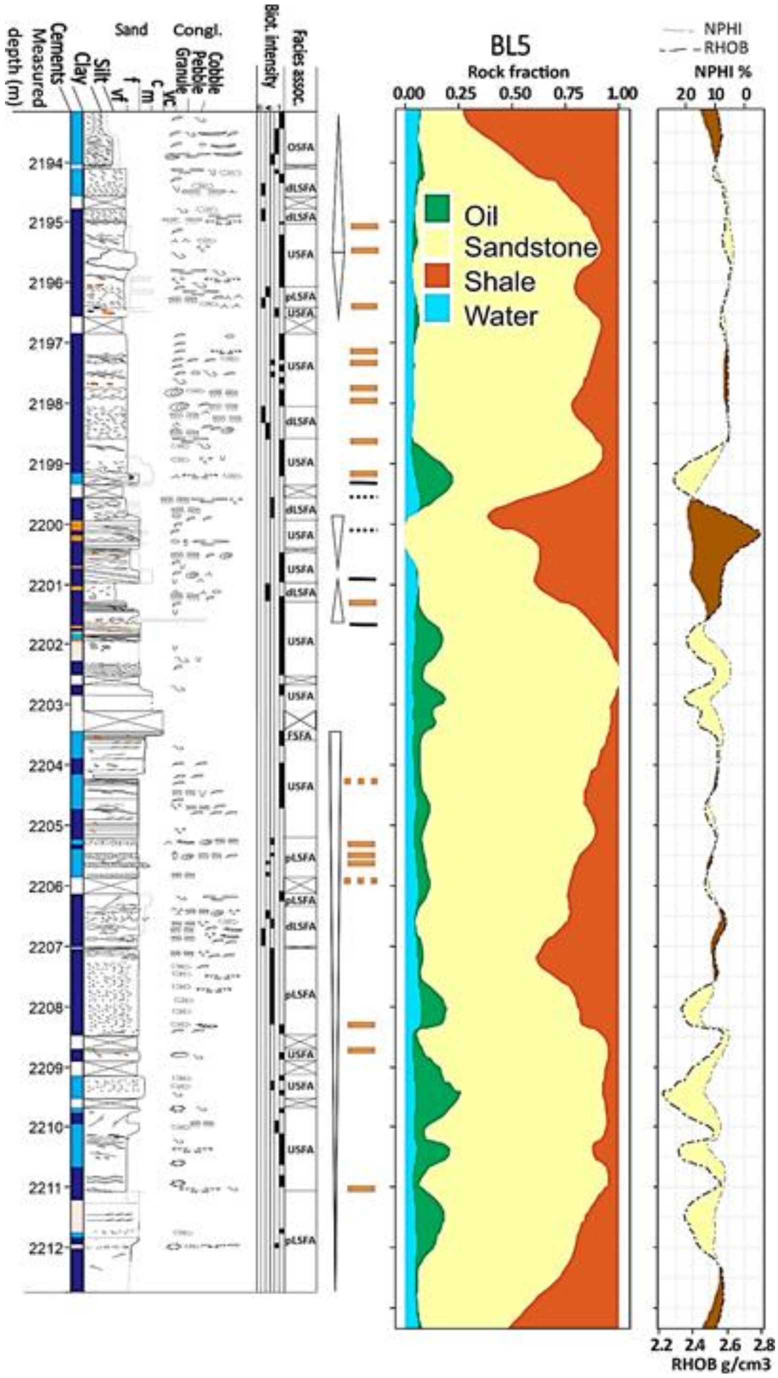

Fig. 8: Schematic section across the Palmers Wood and Bletchingley fields, showing the stratigraphic framework from the Oxfordian to Early Kimmeridgian. The Corallian argillaceous section is succeeded by highstand conditions and deposition of the Corallian sandstones. The highstand conditions were interrupted by a rise in base level before the resumption of highstand conditions. The Corallian is succeeded by the Kimmeridge Clay Formation deposited during resumption of transgression. The section shows about 14.02 m of Corallian sandstones in BL-5, 9.14 m in PW3 and 9.44 m in PW7. Correlation shows that BL5 has an extra sand and mud package in its upper section. The extra sand package shows lower reservoir quality than the other sand packages.

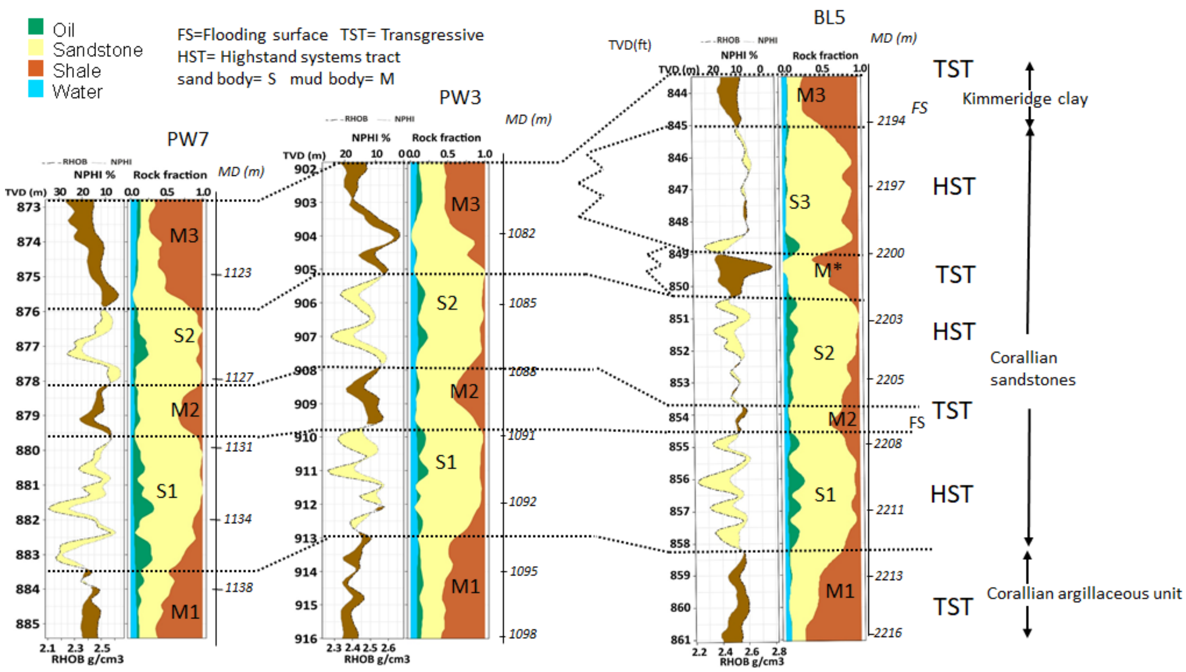

Fig. 9: Integration of sedimentary logs (Figs 5, 6 and 7) and gamma log data from the three wells with correlation of facies associations. The panel correlates erosional and non-depositional (hiatal) discontinuities across the Palmers Wood wells at the boundaries of facies associations. These discontinuities do not correlate to BL5. The Corallian section is thicker in BL5 than the Palmers Wood wells, with the top section of BL5 showing non-contiguous successions of facies associations possibly suggesting that the normal fault separating the two fields underwent syn-depositional movement. The question marks in the upper section of BL5 indicates the sand package S3 (Fig. 8) which do not correlate to the other sand packages/facies associations in PW3 and PW7.

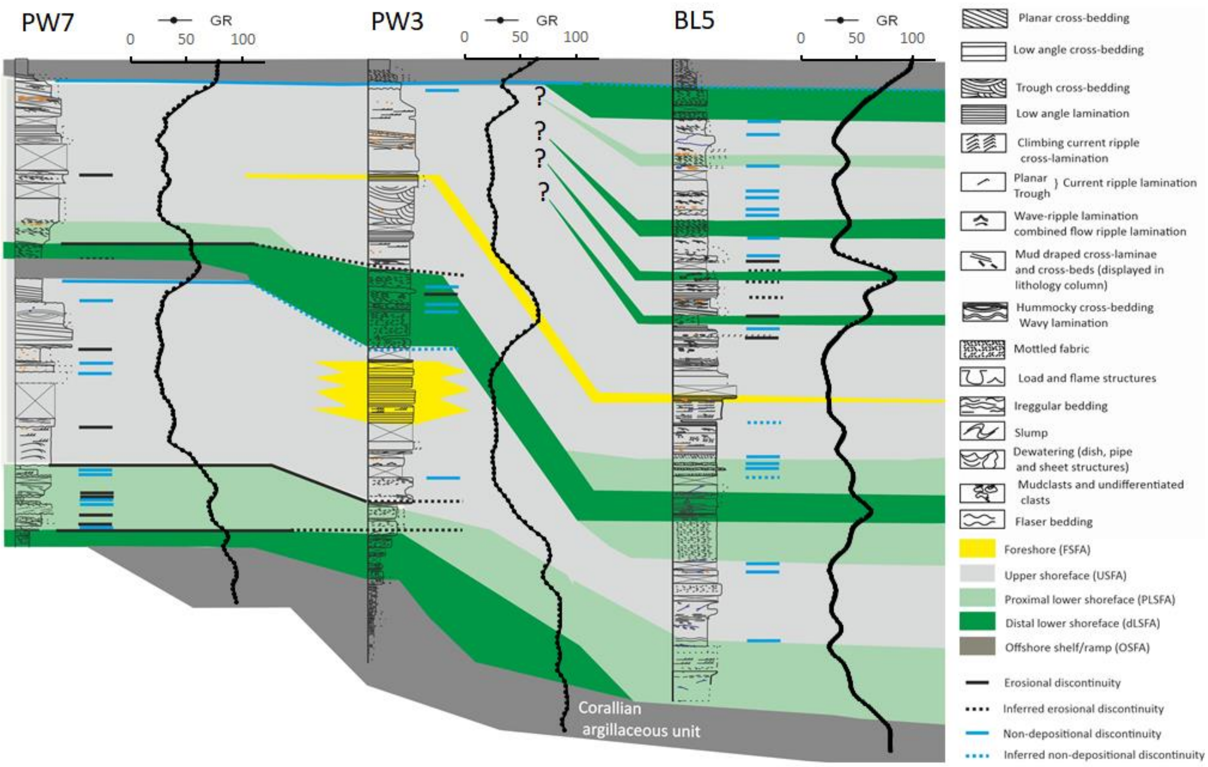

Fig. 10: (A) PW3 (1091.5 m), optical image of medium- to coarse-grained foreshore sandstone. Calcite cementation is intense with cements around grain surfaces typical of phreatic conditions. Aligned, neomorphosed bivalve shells are outlined by earlier-formed micrite envelopes. (B) is an SEM-EDS image of the rectangle outlined in (A), it shows pervasive calcite cementation. (C) is an optical image of a highly calcite cemented, upper shoreface sandstone from PW7 (1130.0 m). Like (A), bivalve shells are aligned suggesting deposition from suspension during relatively low energy conditions. Also, bivalve shells (e.g., top-left and top-right) have acicular calcite cement lining (D) is also an SEM-EDS image of PW7 (1130.0 m) showing dominant calcite cement with some dolomite cement. Quartz (Qtz), calcite (Cal), bivalve (bi) shells, siderite (sid).

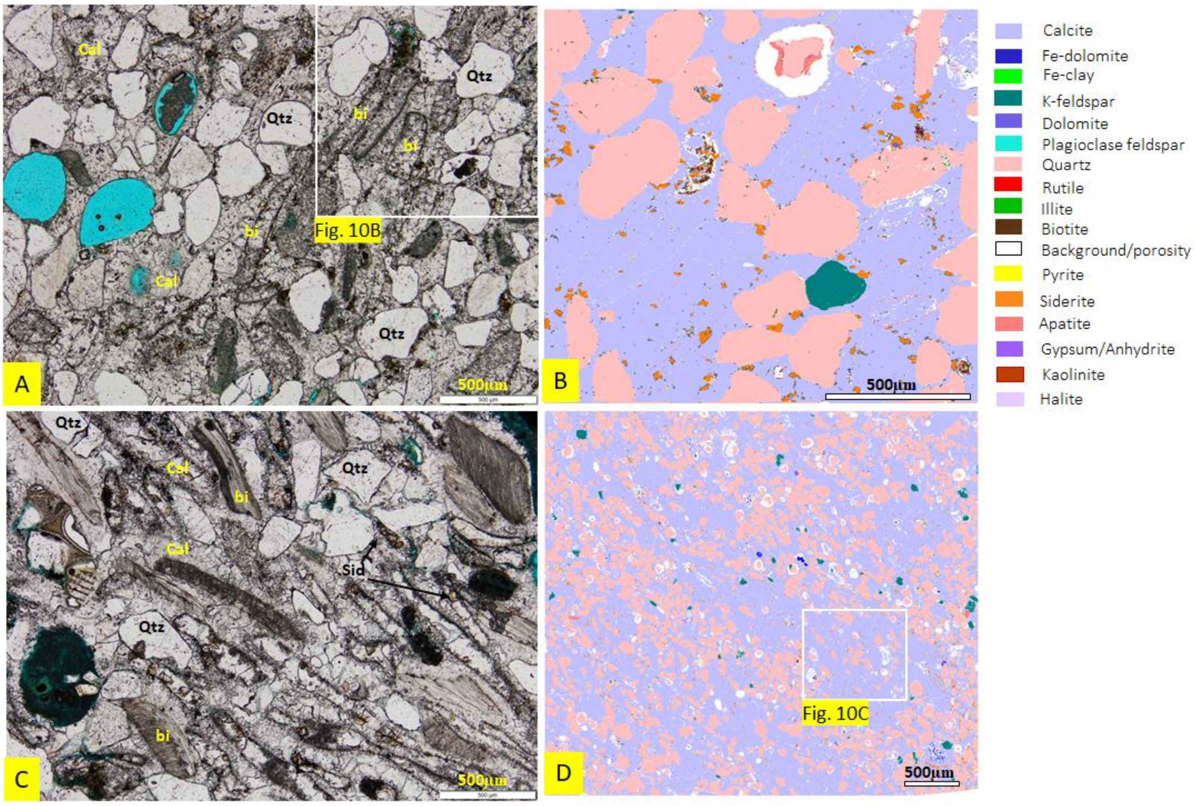

Fig. 11: (A) This is an optical image of proximal lower shoreface sandstone PW3 (1137.4 m) showing fine grained sandstone with high porosity. Bivalve shells are not common compared to Figure 10. (B) represents an SEM-EDS image (area of A highlighted in the rectangle). The thin laminae could either be mud drapes or the lining from burrowing organisms. (C) is a distal lower shoreface sandstone from BL5 (2199.9 m) showing Fe-ooids cemented in calcite cement. The degraded Fe-ooids are recognised by their oval shape and relics of their laminae around detrital grains (centre and bottom-left of image). Some of the Fe-clay has recrystallised to fill pores as seen in the top-centre of Fig.11C (D) is another image of BL5 (2199.9 m) showing siderite matrix, fine-grained quartz and kaolinite, suggesting that sediment was sourced from an iron-rich, extensively-weathered environment. Quartz (Qtz), kaolinite (ka)

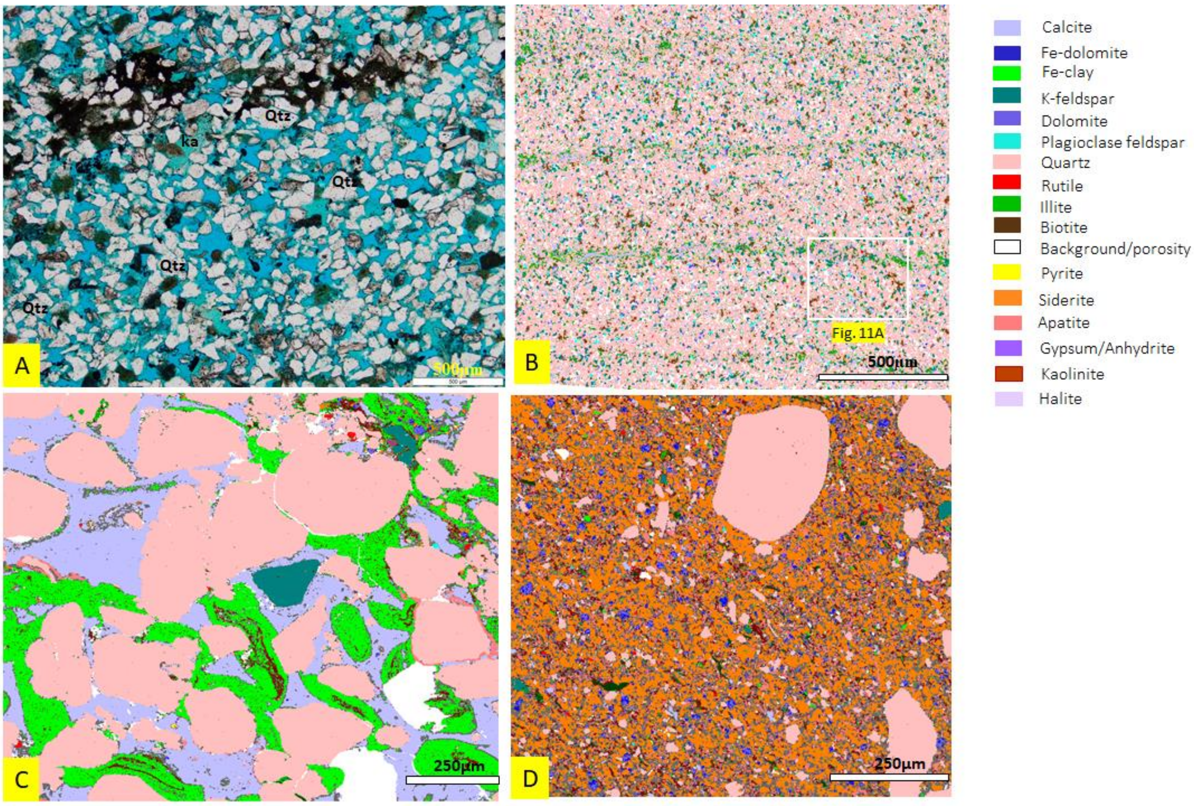

Fig. 12: Data from PW7 1122.5 m which is an offshore clay-rich siltstone. In (A), the dark areas are detrital clay which is distributed throughout the optical image. The bivalve shell in the centre is highly micritised and calcite cement and clay minerals can be seen filling pore spaces. (B) is an SEM-EDS image revealing the highly bioturbated characteristics of the sediment and includes the area of Figure 12A. The SEM-EDS image shows that bivalve clasts are not common in this section and the detrital clay material is mostly composed of illite, with some kaolinite. Some medium grained sand grains are also found within the section suggesting energy conditions were not exclusively low during deposition. (C) Ternary plot, after McBride (1963), showing the relative proportion of quartz (Q) feldspars (F) and lithic grains (L). The plot shows a dominance of a quartz-rich lithology representing a quartz-arenite with minor subarkosic and sublitharenites. Quartz (Qtz), calcite (Cal), bivalve (bi) shells, siderite (sid).

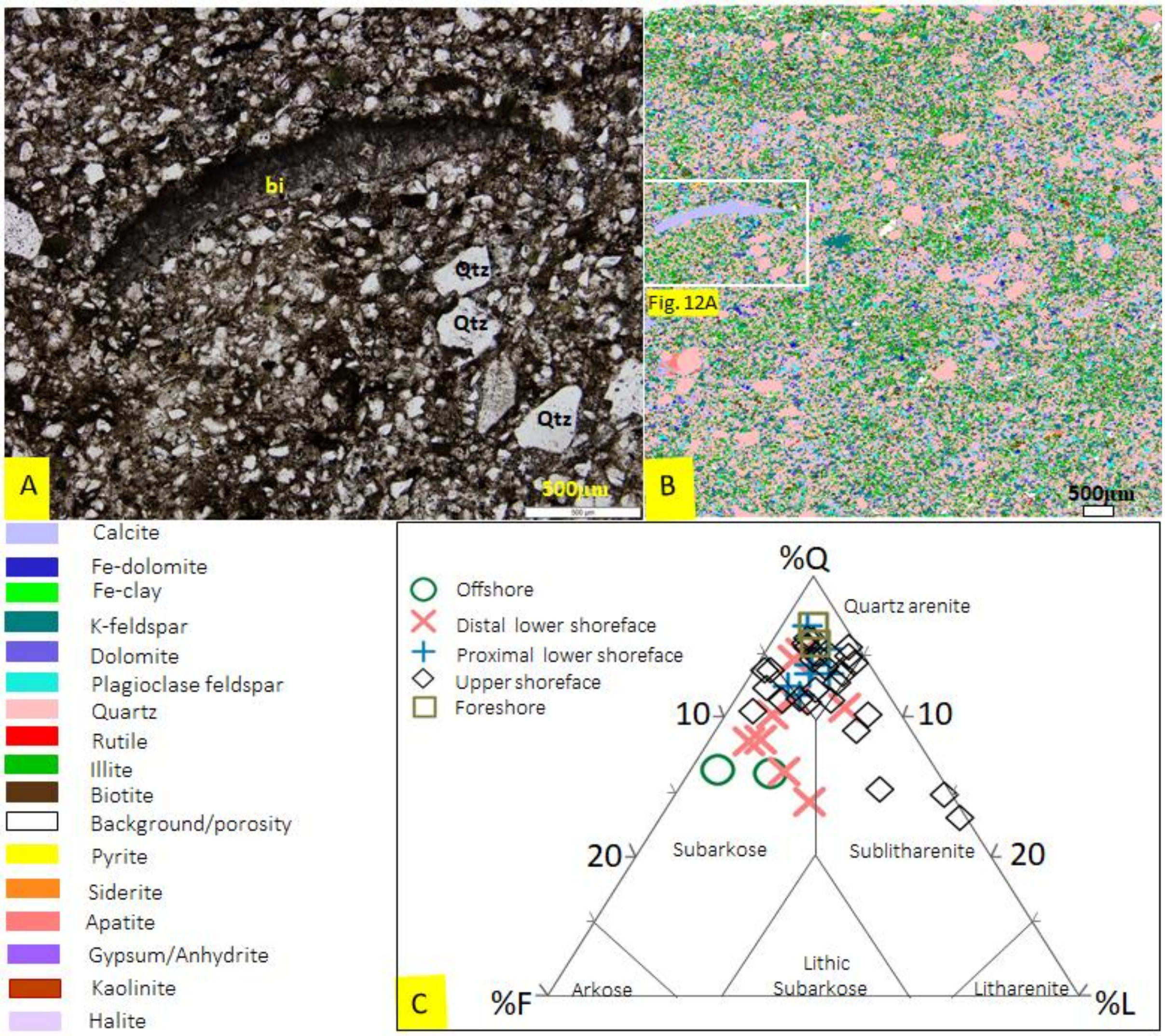

Fig. 13: Boxplots comparing density porosity by facies associations for PW7, PW3 and BL5 (A), calcite content for PW7, PW3 and BL5 (B), clay content for PW7, PW3 and BL5 (C), and percentage of bioclasts for PW7, PW3 and BL5 (D).

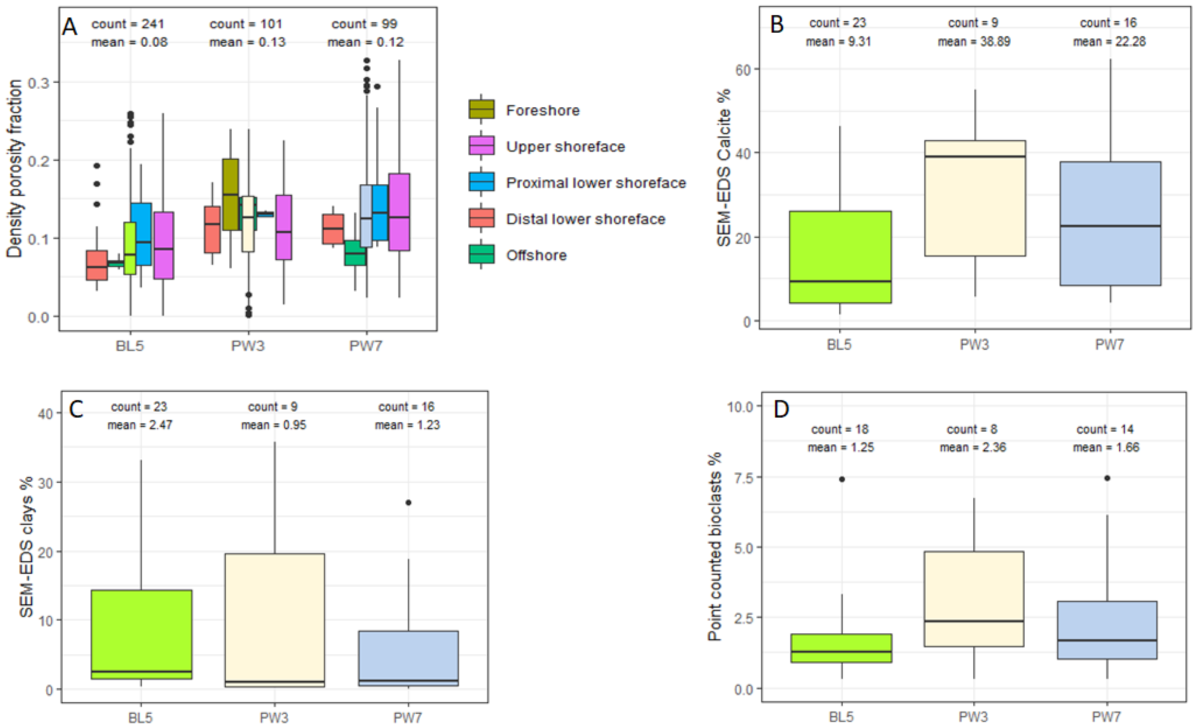

Fig. 14: Depositional model for the Corallian sandstones showing sediment source and increase of water depth across the main fault separating Palmers Wood and Bletchingley.

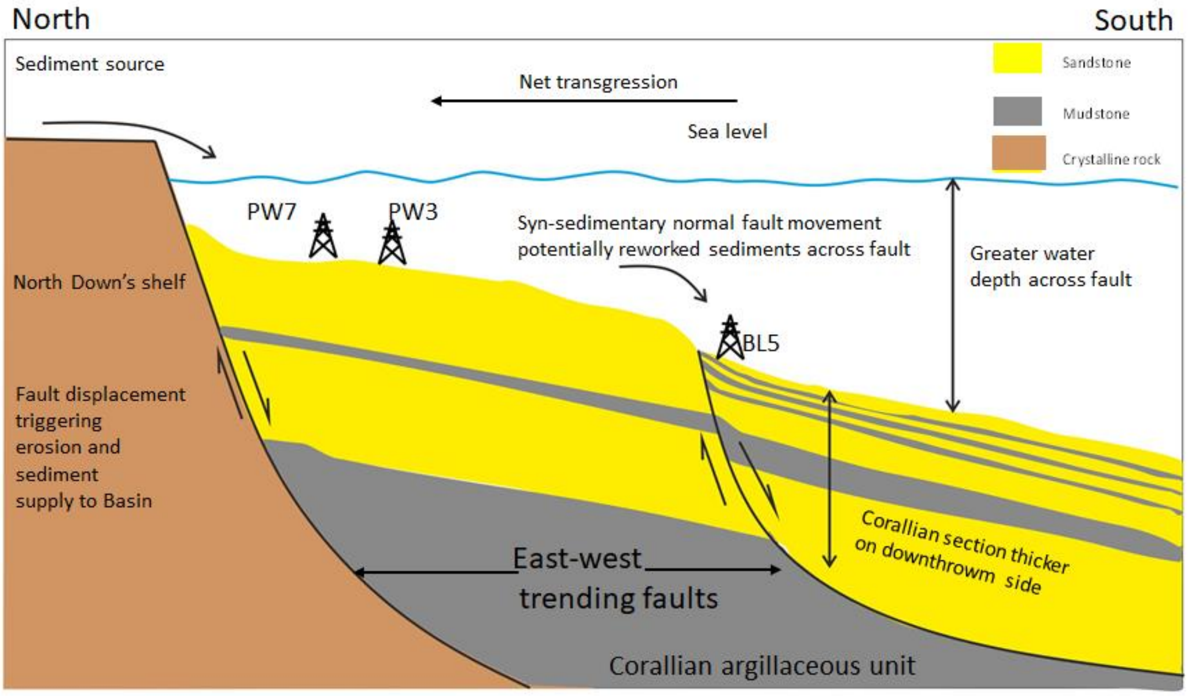

Tables

Table 1: Table showing facies in the Corallian sandstone. The number and variety of facies indicates deposition under a wide range of hydrodynamic conditions.

S/n	Lithofacies	Interpretation
1	Cross-laminated sandstone (S xl)	Upper flow regime deposition
2	Trough-laminated sandstone (S tl)	Deposited by migrating subaqueous 3D ripples
3	Planar laminated sandstone (S pl)	Deposited by migrating subaqueous 2D ripples, high sedimentation rates
4	Wave/ combined flow ripple-laminated sandstone (S r-lam)	Deposited by migrating wave generated 2D ripples
5	Planar cross-bedded sandstone (S px)	Deposited by migrating 2D dunes
6	Trough cross-bedded sandstones (S tx)	Deposited by migrating 3D dunes
7	Massive bedded sandstone (S m)	Formed by rapidly deposited sand
8	Hummocky cross-bedded sandstone (S hx)	High energy storm deposited sandstone
9	Swaley cross-stratified sandstone (S sw)	Deposited during high energy uni-directional wave action
10	Bioturbated/mottled sandstone (S biot)	Deposited from high energy conditions followed by low energy regime conducive enough for organisms
11	Bioturbated/mottled siltstone (Sl biot)	Deposition from suspension , shortly disturbed by organisms
12	Lenticular bedded sandstone/siltstone (s M I)	High energy injection interrupting low energy sand-starved conditions
13	Sandstone/siltstone-mudstone intercalations (S/M)	Rapid changes in energy/sediment supply
14	Low-angle laminated siltstone (Sl x)	Deposition from suspension
15	Trough ripple laminated siltstone (Sl tr-lam)	Deposition by migrating 3D ripples
16	Planar ripple laminated siltstone (Sl r-lam)	Deposition by migrating 2D ripples
17	Mudstone (massive, silty) (M m)	Suspension deposits below wave base representing deposition in a low energy offshore setting.

Table 2: Summary of facies associations, based on a modified version of the facies associations described by Hampson (2003). The facies associations are grouped on the basis of lithology, sedimentary structures and ichnology.

Facies association	**Lithology and sedimentary structures**	**Bioturbation**
1. Foreshore (FSFA)	Low angle Planar-parallel laminated, fine to medium-grained sandstone, commonly highly cemented.	Absent, rare *Macaronichnus.*
2. Upper shoreface (USFA)	Upper-fine to medium-grained sandstone. Low angle cross beds, trough and tabular cross-bedded with minor planar lamination and hummocky cross-stratification. Cementation is variable.	Sparse to moderate (*Ophiomorpha, Skolithos, Planolites, Cylindrichnus some Anchonichnus and Macaronichnus*)
3. Proximal lower shoreface (pLSFA)	Very-fine to fine-grained amalgamated sandstone beds. Hummocky cross-stratification, wave ripple cross-lamination, current ripple lamination, mud-drapes. Cementation is variable.	Moderate to intense (*Anconichnus, Ophiomorpha, Palaeophycus, Rhizocorallium, Arenicolites*, some Cyclindrichnus, *Teichichnus rectus, Thalasinoides and Chondrites* in argillaceous zones)
4. Distal lower shoreface (dLSFA)	Clayey siltstone and sandstone with some fine to medium-grained sand. Beds are non-amalgamated with hummocky cross-stratification, minor wavy lamination and wave ripple cross-lamination. Cementation is variable.	Moderate to intense (*Anchonichnus, Chondrites, Ophiomorpha, Planolites, Palaeophycus, Rosellia, Rhizocorallium, Terebellina, Arenicolites, Teichichnus rectus, Thalasinoides*)
5. Offshore shelf/ramp (OSFA)	Mudstone, silty mudstone, siltstone with some beds of very fine-to upper fine-grained sandstone. Wave ripple lamination, current ripple lamination, lenticular beds, sand-mud heterolithics beds. Cementation is variable.	Intense (*Chondrites, Cylindrichnus, Planolites, Paleophycus, Terebellina, Teichichnus zig-zag, Teichichnus rectus, Thalasinoides* some *Rhizocorallium*)